CERN – EUROPEAN ORGANIZATION FOR NUCLEAR RESEARCH

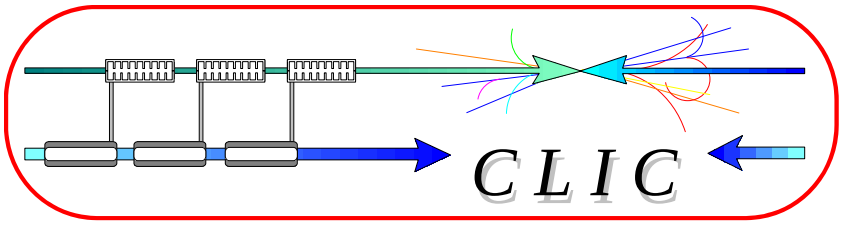

CLIC Note - 776

SUMMARY OF THE BDS AND MDI CLIC08 WORKING GROUP

R. Tomás[1], E. Adli[1], I. Ahmed[2], P.K. Ambatu[3], D. Angal-Kalinin[4], R. Barlow[4&6], J.P. Baud[5], B. Bolzon[5], H. Braun[1], H. Burkhardt[1], G.C. Burt[4], R. Corsini[1], B. Dalena[1], A.C. Dexter[3], V. Dolgashev[7], K. Elsener[1], J.L. Fernandez Hernando[4], G. Gaillard[5], N. Geffroy[5], F. Jackson[4], A. Jeremie[5], R.M. Jones[4&6], P. McIntosh[8], K. Moffeit[7], F. Peltier[5], J. Resta López[9], G. Rumolo[1], D. Schulte[1], A. Seryi[7], A. Toader[4&6] and F. Zimmermann[1]

[1]CERN, [2] NCP, [3] University of Lancaster, [4] CI, [5] LAPP, [6] University of Manchester, [7] SLAC, [8] ASTeC and [9] University of Oxford

CERN-OPEN-2009-018
17/10/2008

Abstract

This note summarizes the presentations held within the Beam Delivery System and Machine Detector Interface working group of the CLIC08 workshop [1]. The written contributions have been provided by the presenters on a voluntary basis.

Geneva, Switzerland
23/09/2009

Contents

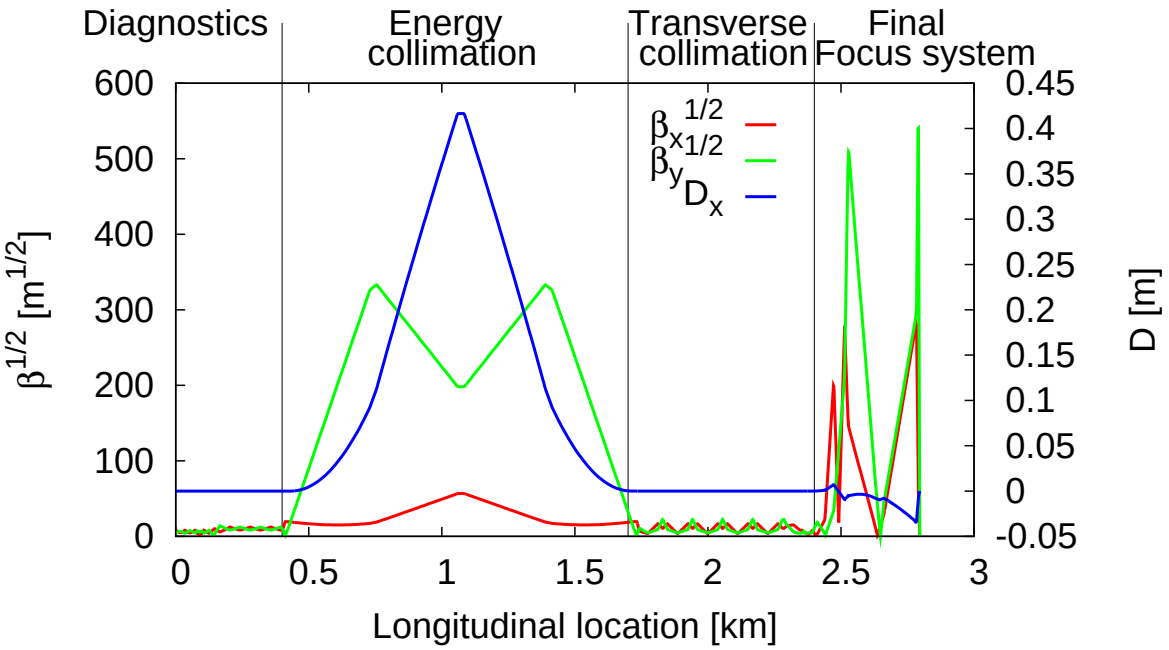

Figure 1: Current CLIC BDS optics.

1 Status of the CLIC Beam Delivery System

Presenter: Rogelio Tomás, CERN

Since 2005 the CLIC Beam Delivery System (BDS) is undergoing different modifications both to maximize its performance and to incorporate all the required instrumentation [2]. A web repository containing current and old lattices can be found in [3]. The optics of the latest CLIC BDS are displayed in Fig. 1. A total length of 2750m harvests the diagnotics, collimation and final focus sections. In the following we discuss the diagnostics and the FFS sections, followed by a brief overview of collective effects and apertures in the BDS. The collimation section is reviwed in section 9.

1.1 Diagnostics section

The diagnostics section serves to correct the transverse coupling and measure the transverse beam emittance. Simulations performed by I. Agapov suggest that a relative error of 7% is expected in both transverse emittances, assuming the passge of 3 identical trains and a beam-size measurement with a 10% relative error at three laser wires. The design vertical beam size at these laser wires is 1μm. As suggested in [4] the backscattered electrons at the laser wires are a better signal than the forward photons. These electrons are collected

The energy measurement has been devised in a way to minimize the required space due to the tight constrains on the CLIC total length. The deflection of the first dipole in the collimation section together with high precission BPMs provides the most compact energy measurement. A conceptual layout is shown in Fig. 2. The energy measurement resolution of the set-up is estimated to be 0.04%. The integrated magnetic field is assumed to have a calibration error of 0.01% and the BPM resolution is 100nm.

An upstream polarization measurement has been fully devised for the first time in [5]. A drift space between the collimation dipoles was found to be an ideal location for the polarimeter being long enough and properly aligned to the IP direction.

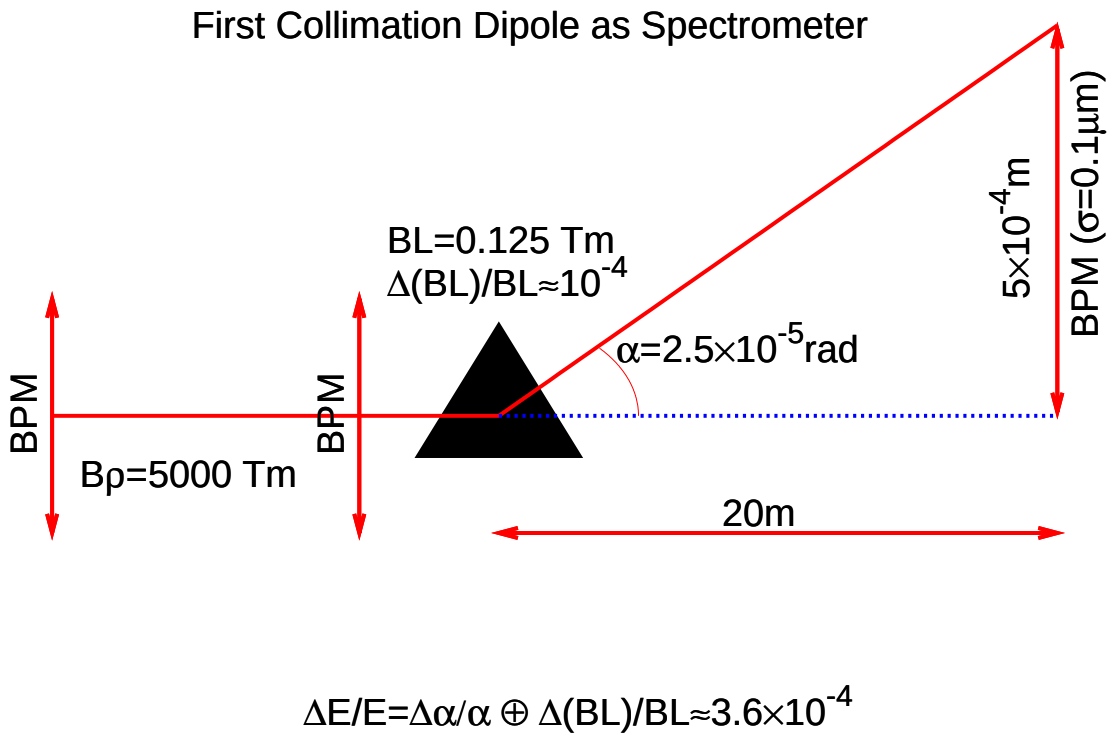

Figure 2: Conceptual compact CLIC energy measurement.

1.2 Final Focus System

The current FFS optics is shown in Fig. 3. This optics corresponds to a L^*=3.5m. Previously the CLIC L^* was 4.3m, going to a shorter L^* slightly improved the luminosity bandwidth 4 and reduced the required number of non-linear correctors keeping the same luminosity [2]. An extra advantage of the L^*=3.5m compared to the 4.3m case is the need of a shorter length by 100m.

Synchrotron radiation effects have a large impact on the performance of the CLIC FFS. A detailed review of this phenomenon is given in Section 6.

When assigning realistic errors to the FFS magnetic elements the performance is severely deteriorated. Tuning the FFS consists in varying all available parameters until the performance reaches a satistactory level. Tuning simulations have been performed for a statistichal ensamble of machines yielding the final relative luminosity as shown in Fig. 5. About 20% of the cases end with a luminosity lower than 80% of the design. This situation should be improved by using better tuning algorithms, profitting from the future ATF2 experience.

1.3 Collective effects

Four collective phenomena have been recently evaluated for the BDS:

- **Ion instability**. Residual gas ionization is caused both by direct ionization of the e^--molecules collisions and by field ionization. Simulations from G. Rumolo have shown that ion instability does not develop for a 10 nTorr vacuum. Field ionization has not been studied yet.
- **Resistive wall wakefields**. Fig. 6 shows the excursion of the last bunch of the train due to the resistive wall wakefield as a function of the longitudinal location in the CLIC

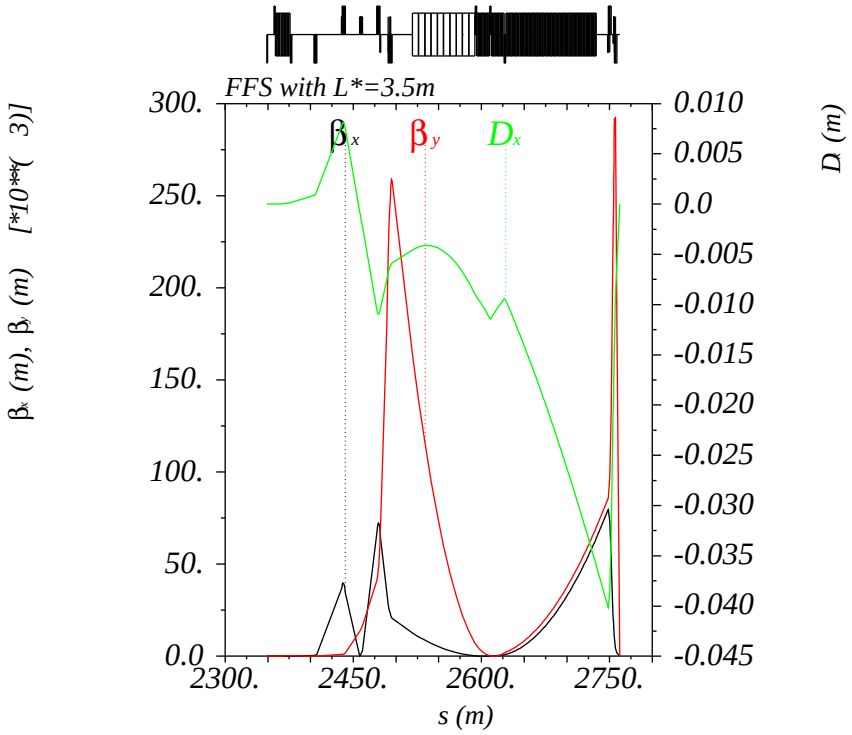

Figure 3: CLIC Final Focus System with $L^* = 3.5$m.

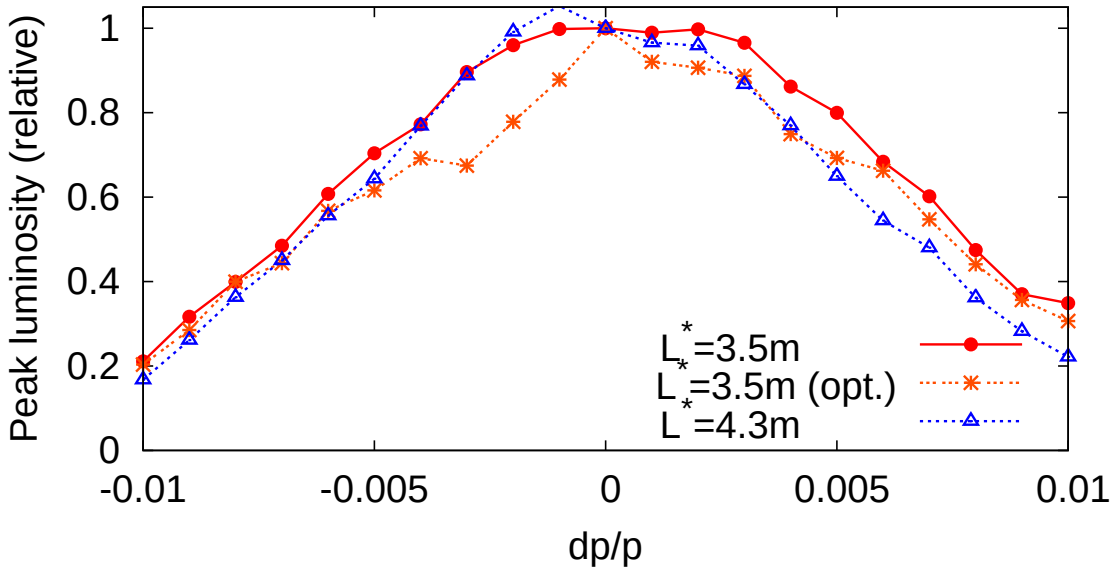

Figure 4: Luminosity bandwith of two FFS with 3.5m and 4.5m L^* respectively. The bandwidth of the system with shorther L^* is slightly larger.

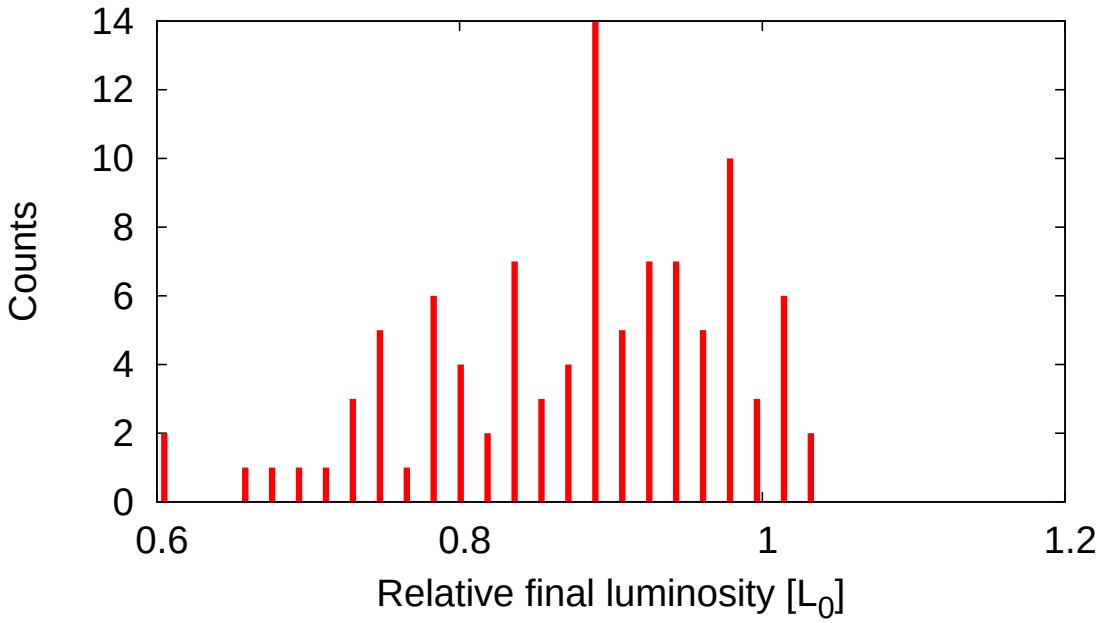

Figure 5: Histogram of relative luminosity after assuming realistic errors and tuning for a maximum number of 18000 iterations.

BDS for different beam-pipe radii. The effect of this wakefield decreases for increasing radius and from the plot we conclude that at 8mm the effect becomes negligible. This number sets the reference aperture for the BDS as discussed below.

– **Collimator wakefields**. Alignment and jitter tolerances arising from the collimator wakefield kicks are computed in Section 9. However, the validity of the analytical equations has never been experimentally verified due to the very short bunch length.
– **Coherent synchrotron radiation**. E. Adli has confirmed via simulations that the coherent synchrotron radiation has a negligible effect in the CLIC BDS. This is also observed by the approximate calculation of the average energy loss due to this effect:

$$\delta E \approx \frac{r_e q L E_0}{e\gamma (R^2 \sigma_s^4)^{1/3}} \approx 1\ MeV \tag{1}$$

1.4 Apertures

As mentioned above the reference BDS beam-pipe radius is set to 8mm to avoid resistive wall wakefields. It has been verified that conventional technology can be used to build all magntes of the collimation section.The FFS becomes more problematic in terms of apertures and magnet technology. In particular the final quadrupoles, see Table 1, require smaller apertures than the 8mm and have larger gradients than previous designs [6] due to the enlarged vertical emittance and the reduction of β^*. A beam pipe radius of 1mm has been assumed in the computation of the apertures. This thickness could be relaxed with magnet designs including the beam-pipe. If the magnet design proves unrealistic or the aperture has an impact on performance due to collective effects there are two possible solutions: increasing the length of the quadrupoles or increasing the β^*.

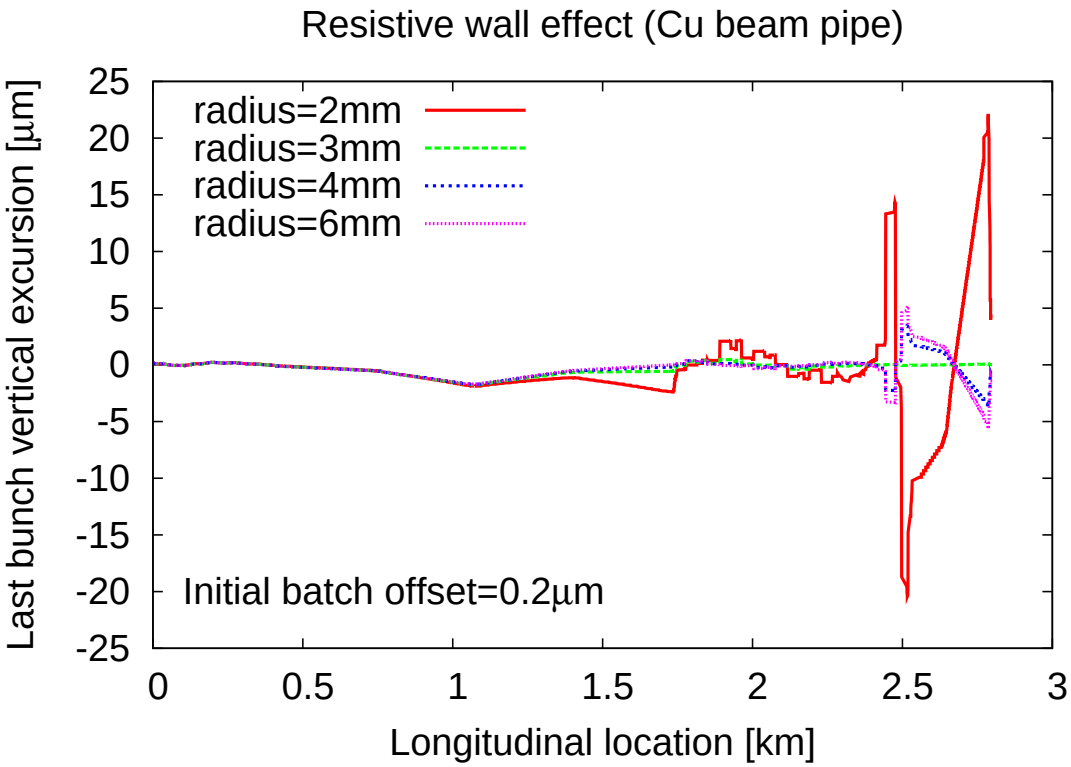

Figure 6: Excursion of the last bunch of the train due to the resistive wall wakefield as a function of the longitudinal location in the CLIC BDS for different beam-pipe radius.

	Unit	L*=3.5m		L*=4.3m	
		QF1	QD0	QF1	QD0
Gradient	T/m	200	-575	133	-382
Length	m	3.26	2.73	4.0	3.3
Aperture (radius)	mm	4.69	3.83	6.67	6.76
Outer radius	mm	-	< 35	-	< 43
Peak field	T	0.94	2.20	0.89	2.58
Field stability	$\frac{\Delta k}{k} 10^{-4}$	0.3	0.08	0.3	0.08
Octupolar error	10^6T/m^3	-	< 1	-	< 0.5
Dodec. error	10^{16}T/m^5	-	< 2	-	< 1.0

Table 1: Technical specifications for the final quadrupoles.

2 ATF2 Ultra-low betas proposal

Presenter: Frank Zimmermann, CERN

The CLIC parameters at 500GeV have been chosen to be *conservative,* meaning that they ought to be supported by experience in real machines (past or ongoing like ATF2). In particular the 500GeV CLIC IP beta functions are ($\beta_x,\ \beta_y$)=(10, 0.2)mm with L*=4.3m while the nominal ATF2 IP betas are ($\beta_x,\ \beta_y$)=(4, 0.1)mm for L*=1m. The chromaticity scales roughly with L$^*/\beta^*$ and therefore the 500GeV CLIC is a factor 2 more chromatic than ATF2. For this reason we propose to test at least a factor 2 reduction in the horizontal and vertical IP beta functions of ATF2. A summary of the relevant parameters of the different projects is given in Table 2 including a more precise computation of chromaticity to confirm the rough scaling law mentioned above for similar FFS. The FFTB had a totally different design, thus its larger chromaticity than the new FFSs. A pushed ATF2 is the only way to prove the feasibility of the CLIC 500GeV chromatic level. The CLIC 3TeV option is more ambitious and has a $\beta_y^* = 0.09$mm. To prove this chromatic level, ATF2 β_y^* should be reduced by another factor of 2 (factor of 4 from nominal). This might require new or modified hardware and instrumentation.

The ILC project would also largely benefit from this test, in particular by gaining experience in exploring lower betas and facing increased tuning difficulties for this pushed machine.

Reference [7] studies a wide range of ATF2 β^* values. The larger β^* are useful during the commissioning period in order to reduce the difficulty of the system. The previous study also shows that there is some margin to lower the vertical IP beta function. Figure 7 shows the vertical sigma versus the vertical beta functions without including radiation effects. A minimum beam size of 20nm seems possible with the magnets and power supplies presently planned in the beam line (not considering potentially increased bremstrahlung background in the Shintake monitor from reducing β_x). Lattice aberrations dominate in the lower betas regime. Codes as MAPCLASS [8] could be used to further investigate the compensation of the lattice aberrations. The nominal ATF2 is just a factor of two away from the 500GeV CLIC in terms of chromatic behavior.

There is another important aspect determining the feasibility of an FFS: the tuning difficulty. By tuning we understand the process of bringing the system to its ideal performance under realistic conditions of lattice errors (misalignments, multipole errors, mispowerings, etc). The tuning difficulty should roughly scale inversely to the beam size at the IP. Achieving the CLIC IP beam sizes in ATF2 is not possible due to the difference in geometrical emittance but the strategy should be reducing the ATF2 betas to the lowest feasible values and experience with the increased tuning difficulty can be extrapolated to both CLIC and ILC. An ATF2 tuning simulation is shown in Fig. 8 for the case with $\beta_y = 0.05$mm. 90% of the seeds converge to a satisfactory beam size while 10% finished at larger beam sizes.

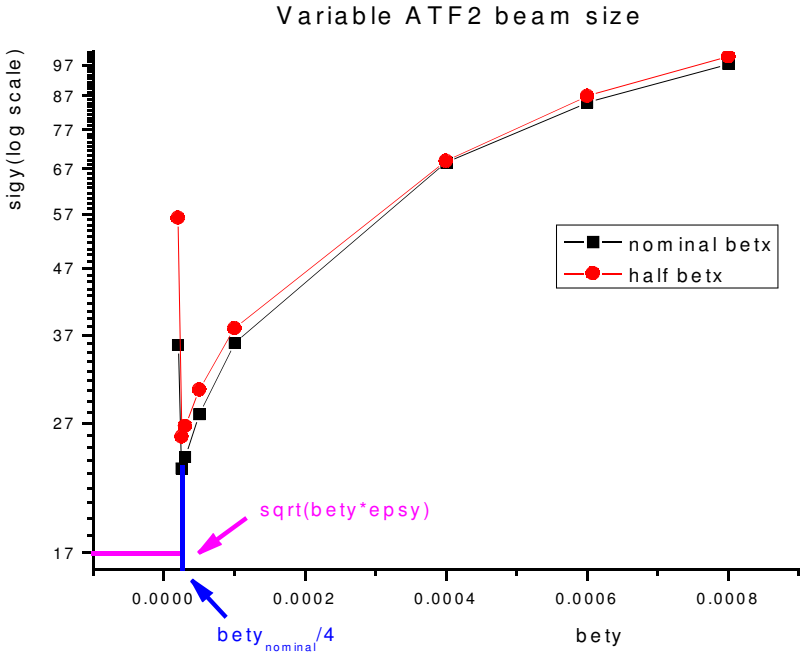

Figure 7: Vertical beam size (in [nm]) at the IP versus vertical beta function (in [m]) for two cases: nominal and half horizo ntal beta functions. Aberrations change the ideal trend of this curve for the very low betas and they are larger for the case with half the nominal horizontal beta. The quarter of β_y is marked on the plot together with the corresponding ideal vertical sigma.

Project	Status	β_y^* [mm]	L* [m]	L$^*/\beta_y^*$	ξ_y
FFTB	Design	0.1	0.4	4000	17000
FFTB	Measured	0.167	0.4	2400	10000
ATF2	Design	0.1	1.0	10000	19000
ATF2 pushed	Proposed	0.05	1.0	20000	38000
ATF2 ultra-low	Proposed	0.025	1.0	40000	76000
CLIC 500GeV	Design	0.2	4.3	21500	35000
CLIC 3TeV	Design	0.09	3.5	39000	63000
ILC	Design	0.4	3.5	8750	15000
ILC pushed	Design	0.2	3.5	17500	30000

Table 2: Relevant parameters of the different projects [9, 10, 11, 12]. ξ_y is a precise computation of natural chromaticity given by $(T_{346}R_{33} - T_{336}R_{34})/\sqrt{\beta_y^*}$. This is shown on the table to verify that the chromaticity of similar FFSs roughly scales with L$^*/\beta_y^*$, the FFTB being the only FFS having a totally different design.

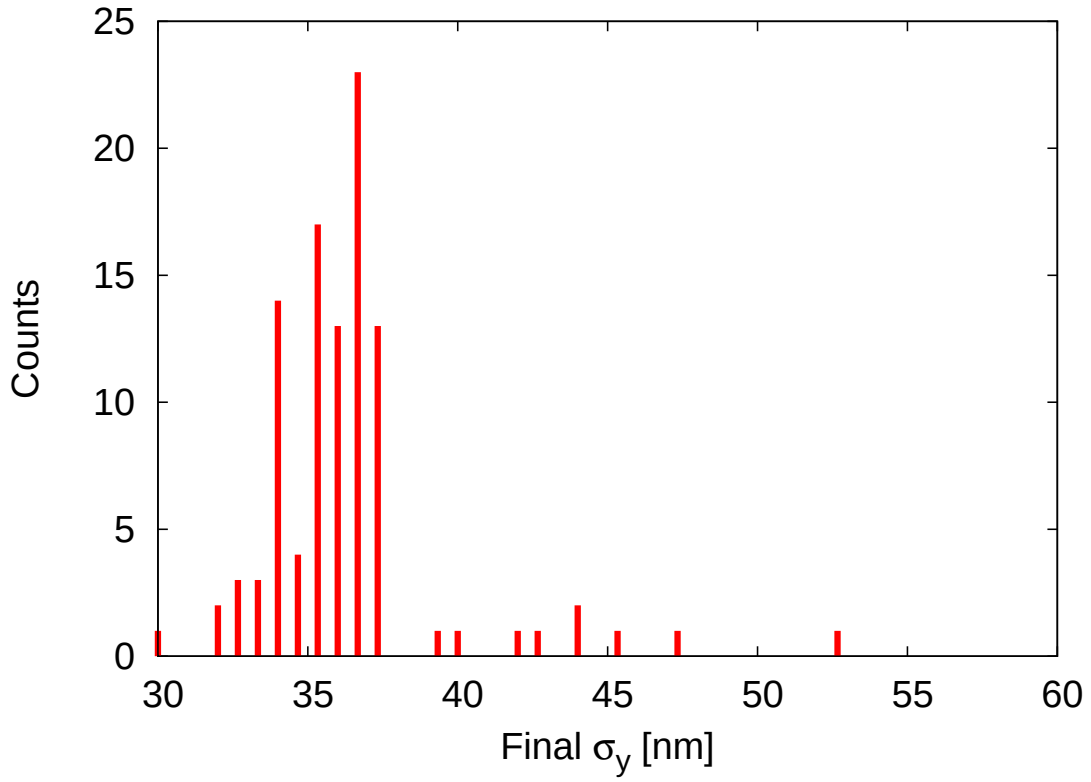

Figure 8: Histogram of the ATF2 vertical beam sizes at the IP for the case with $\beta_y^* = 0.05$mm, for 100 seeds with initial errors and after tuning for no more than 10000 iterations.

3 Near IR FF design including FD and longer L* issues

Presenter: Andrei Seryi, SLAC

The ILC approach to stability of Final Doublet is based on possibility to apply intratrain feedback within the 1ms long train, which allow avoiding any active mechanical stabilization of FD and allow to tolerate FD jitter of the order of hundred nm. The kicker of the intratrain feedback in ILC is located between QD0 and QF1, about 10m from IP.

For CLIC, with 1nm beam size and 150ns train, one has to use all possible options to provide stability of FD. Therefore, one cannot afford 50ns trip-around time of intra-train feedback, and one has to minimize the trip-around time, thus one has to move kicker and BPM of the intratrain feedback closer to the IP. Let us assume that we can place the kicker and BPM 2m from IP, which will give irreducible delay of 12ns. Electronic latency may give another 13ns [13], giving 25ns latency in total, which would allow about six iterations of intratrain feedback in total.

Placing the feedback kicker, BPM and the electronics (which may require shielding) may require some increase of L*, so it is likely that FD will be partly outside of the detector. Stability of the latter is important – it was observed at SLD that stability of its superconducting triplets was about 30nm, while stability of the floor was about a nanometer in the same frequency range. While SLD was not designed to be stable, this comparison is indicative – the tunnel floor is likely to be much more stable than the detector. It gives another reason to consider removing FD from the detector entirely, by increasing L* to about 8m, and placing FD on a more stable tunnel floor.

Increasing L* in principle leads to some reduction of luminosity, due to larger chro-

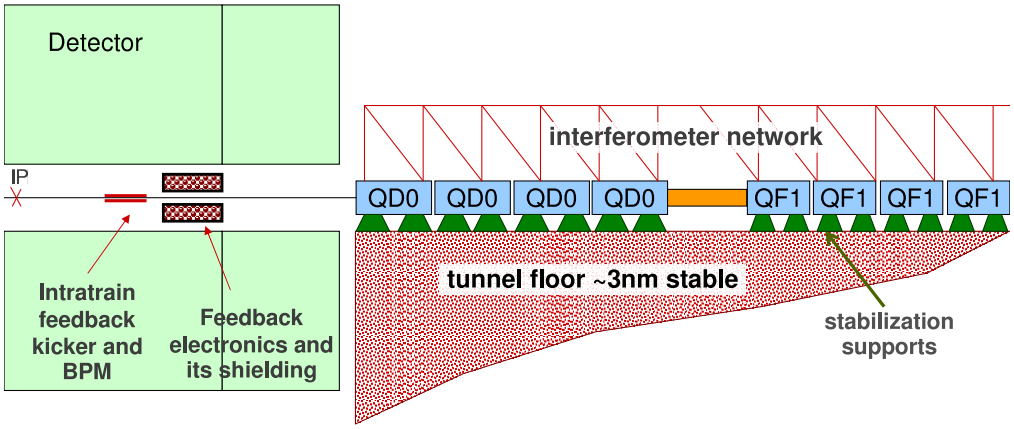

Figure 9: Conceptual approach for CLIC IR with doubled L*. This configuration would simplify achieving the FD stability and also simplify the Machine-Detector Interface.

maticity and potentially larger aberrations. One other potential limitation is tightening if the collimation depth with longer L*, and corresponding increase of jitter amplification and emittance growth due to collimation wakefields. However, if the collimation depth is limited by extraction apertures, and not by the vertex detector, then the increase of L* may be done simultaneously with increase of extraction apertures, without tightening of the collimation depth. In such assumptions, analysis for ILC parameters predicted slow decrease of luminosity with increase of L*. For CLIC case the analysis should be repeated.

For 3TeV CM CLIC, in order to reduce synchrotron radiation effect from FD on the beam size (Oide limit [30]), one may need to lengthen the FD quads, especially QF1. This may suggest that it would be natural to split such long quads to independent pieces, to reduce stability requirements as $1/\sqrt{N}$ (for those frequencies where they will move independently). This will further ease the challenge of FD stability.

Taking all this into account, the CLIC IR with doubled L* may look as shown in Fig. 9, which would have the following advantages: a) reduced feedback latency – several iteration of intratrain feedback over 150ns train; b) FD placed on tunnel floor, which is about ten times more stable than detector – easier for stabilization; c) design is not limited by the sizes of stabilization system or interferometer hardware; d) reduced overall risk and increased feasibility; e) shorter L* may still be consider for an upgrade.

In order to further test the feasibility of such proposal, a tentative version of final focus system with L*=8m was looked at. The design is based on NLC BDS, where the FD was lengthened and dispersion reduced to minimize SR effects at 3TeV CM. Aberrations were reduced but there were still room for further improvements. This optics is shown in Fig. 10.

The optics is designed for 3TeV CM, IP emittances = (660/20) nm and IP betas = (6.9/0.068) mm. The Final Doublet for this optics has the following strength at 3TeV CM: QD0: 213 T/m and QF1: 72T/m, which allow use of SC quads with aperture radius of 1cm. (Which is still smaller than the vertex, so it would not make the collimation depth tighter).

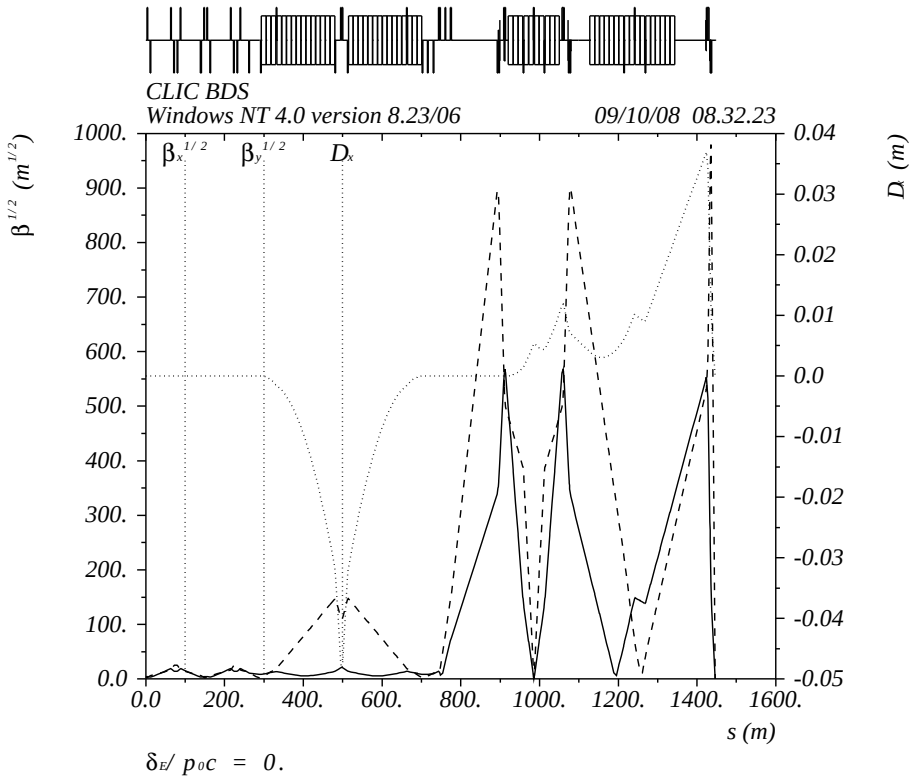

Figure 10: Tentative FFS optics with L*=8m.

There were several 3rd and 4th order aberrations which were still noticeable, which include $U_{xx'x'x'}$ and $W_{yx'x'y'\delta}$.

Evaluation of this optics was done by DIMAD tracking with synchrotron radiation, and then by beam-beam calculation by Guinea-pig, looking at the luminosity in 1% peak of luminosity spectrum. The luminosity achieved so far is: L(1%)= $1.35 \times 10^{34} cm^{-2} s^{-1}$ for nominal (6.9/.068)mm IP betas, however, due to remaining aberrations, higher luminosity L(1%)= $1.60 \times 10^{34} cm^{-2} s^{-1}$ is achieved for increased IP betas: (13/0.1)mm. The latter correspond to 80% of the nominal CLIC luminosity. (However, one needs to take into account that usually CLIC luminosity includes 20% margin to account for various errors).

A tentative conclusion from this very brief study is that a BDS with L*=8m may be feasible for CLIC, even for 3TeV CM. Luminosity (in 1% peak) is close to 80% of the nominal $2 \times 10^{34} cm^{-2} s^{-1}$ (although not including a 20% margin to account for errors). Further optimization may be possible. Advantages of doubled L* are that the FD stability may be claimed to be close to be feasible now, with present technology that was already demonstrated (the FD magnetic center stability is a separate issue independent of L*, and needs to be verified in any case). From the other hand, CLIC FD stability requirements for L*=3.5m are extremely challenging. Plus, longer L* gives much simpler MDI, easier FD design, no need for antisolenoid, etc.

Further work on optimization of the design is planned to be done in close collaboration with CLIC colleagues.

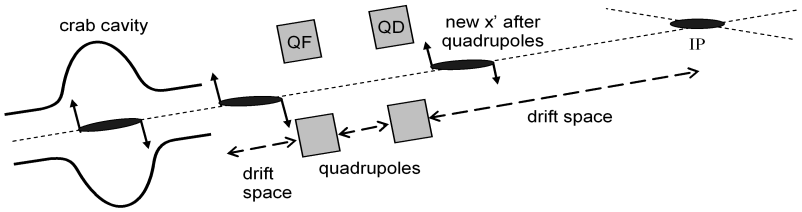

Figure 11: Crab cavity conceptual view.

4 Crab Cavity Development for CLIC

Presenter: Amos Dexter, CI

4.1 Introduction

The current CLIC scheme proposes to collide charged bunches with a horizontal size of 60 nm and a vertical size of 0.7 nm at the interaction point. This size should be compared with the ILC bunch size of 600 nm by 4 nm. Analysis of the final focus undertaken at CERN indicates that a head on collision scheme is impossible with known technology and hence a crossing angle of 20 mrad has been proposed. With such a large crossing angle a crab cavity system is essential in order to achieve the target luminosity. The currently proposed technology for the CLIC linac is 12 GHz copper cavities operating at room temperature. The crab cavity system must operate at this frequency, a harmonic or a suitable sub-harmonic dependent on the number of RF cycles between bunches. Currently the authors are investigating the use of a 12 GHz room temperature copper cavity as it gives complete flexibility of bunch spacing and exploits fabrication technologies under development for the main linac.

4.2 Requirement

The CLIC bunch size and crossing angle dictate that crab cavities will be needed to rotate bunches of particles into alignment at the interaction point if the desired luminosity is to be achieved.

The crab cavity is a deflection cavity operated with a 90^{o} phase shift, its effect is shown in Fig. 11. A particle at the centre of the bunch gets no transverse momentum kick and hence no deflection at the IP. A particle at the front gets a transverse momentum that is equal and opposite to a particle at the back.

It is anticipated that every sixth bucket for the CLIC linac will be filled hence the bunch frequency is 2 GHz. This means that that the crab cavity must operate at either 2 GHz, 3 GHz, 4 GHz, 6 GHz or 12 GHz. Transverse space not be a issue for any of these frequency choices except possibly 2 GHz in conjunction with a superconducting cavity. The availability of longitudinal space is likely to be a few metres maximum.

There are two key issues for the design of any linear collider crab cavity system. The first is achieving a degree of synchronisation between cavity RF phases such that electron and position bunches do not start missing each other in the horizontal plane. The second is wakefields.

Linear collider crab cavities are typically placed immediately before the final focus quadrupoles and hence are in a region of high β. This position minimises the required cavity kick and limits the signalling distance between the cavities so as to assist synchronisation. The most significant wakefield effects are vertical kicks causing bunches to starting missing

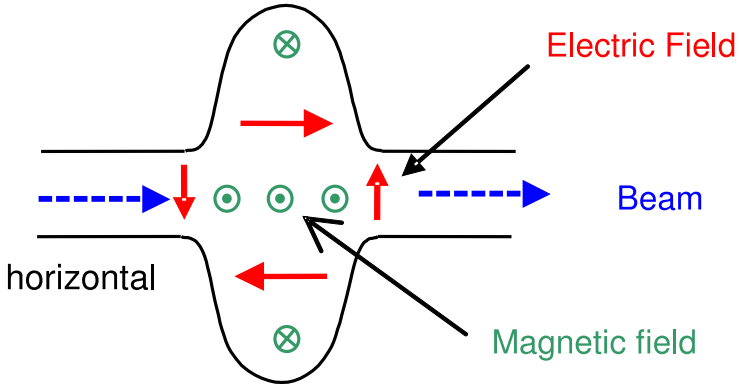

Figure 12: Crab cavity fields view.

each other in the vertical plane. A major part of any crab cavity design is the wakefield damping scheme [14].

A final issue for the crab cavity is flexibility of the power supply [15]. Figure 12 shows the electric and magnetic fields inside a single cell dipole cavity. It is immediately apparent from Fig. 12 that beam loading only occurs when the bunch is off axis and beamloading changes its sign depending on which side of the centre that the beam passes. At the location of the crab cavity bunch offsets can large. In the case of CLIC an estimate is 0.4 mm. At the arrival of each bunch train the power supply does not know whether it will need to deliver power into the cavity or provide a 180^{o} phase shift to assist power leakage from the cavity through a circulator to a load.

4.3 Crab Cavity Equations

Defining the transverse kick at the crab cavity as the transverse momentum imparted divided by the axial momentum we write

$$x_c^{'} = \frac{\Delta p}{\mathrm{mc}} \tag{2}$$

The relation between displacement at IP and transverse kick at the crab cavity is given as

$$x_{\mathrm{ip}} = R_{12} x_c^{'} \tag{3}$$

By nature of the oscillation of an RF field, kick depends on relative time of arrival t and using Eq.(2) is determined by

$$x_c^{'} = \frac{V}{E_o} \sin\left(\omega\ t\right) \tag{4}$$

where the transverse voltage kick is defined from

$$\mathrm{eV} = c\Delta p \tag{5}$$

and

$$\mathrm{eE}_o = \mathrm{mc}^2 \tag{6}$$

The transverse kick includes the transit time factor. Defining Δt as the time difference between a particle that is undeflected and one which is, then combining the above equations the displacement for delayed arrival is given by

$$\Delta x_{\rm ip} = R_{12}\frac{V}{E_o}\ \sin\left(\omega\ \ \Delta t\right) \tag{7}$$

Note that Δt relates to both the timing of the ends of a bunch and the timing of the centre of a late bunch. For small Δt we have

$$\Delta x_{\rm ip} \simeq R_{12}\frac{V}{E_o}\,\omega\ \ \Delta t\ \ (\text{for short bunches or small time errors}) \tag{8}$$

Equation (8) determines the required displacement at the end of a bunch to get the correct crabbing angle. When the cavity field is adjusted for perfect alignment at the IP we have that

$$\Delta x_{\rm ip}\left(t\right)\ =\ \theta_r c\ \Delta t \tag{9}$$

where half the crossing angle $\theta_{\rm r}$ = 0.5 $\theta_{\rm c}$.

The kick voltage V required from system to achieve a rotation angle of $\theta_{\rm r}$ is hence given by

$$\theta_r = \frac{\Delta x_{\rm ip}\left(t_{\rm end}\right)}{c\ \Delta t_{\rm end}} \simeq R_{12}\frac{V}{E_o}\frac{\omega}{c} \tag{10}$$

hence

$$V \simeq \frac{\theta_r E_o c}{\omega\ R_{12}} \tag{11}$$

Comparing the CLIC requirement with the ILC requirement E_o increases by a factor of three, $\theta_{\rm r}$ increases from 14 mrad to 20 mrad but R_{12} increases from 16 m to 25 m hence for an identical frequency of operation the kick increases by a factor of 2.75. It is also apparent from (8) that this kick can be reduced by increasing the frequency. How much power one requires to provide this kick depends on the loaded Q factor of the cavity. For optimum power transfer one matches the loaded Q to worst case beamloading and cavity losses. When a bunches of charge q pass through a dipole cavity with repetition $f_{\rm rep}$, phase ϕ and with offset a the power extracted from the cavity is

$$P_b = \ \ {\rm qV}\left(\frac{a\omega}{c}\right)\ f_{\rm rep}{\rm cos}\varphi \tag{12}$$

Combining Eqs. (11) and (12) at the perfect crabbing phase ϕ = 0 we obtain

$$P_b = \ \frac{a\ \theta_r q\ f_{\rm rep} E_o}{R_{12}} \tag{13}$$

Table 4 computes this peak power requirement for the ILC at 1 TeV centre of mass and for CLIC at 3 TeV centre of mass. Before any consideration of cavity frequency is made one realizes that the CLIC crab cavity will be a high power device.

The key challenge for the RF system is to phase the cavities so that bunches do not miss [16] as illustrated in Fig. 13. The luminosity reduction factor S for Gaussian bunches

	a	½ crossing angle	bunch charge	f repetition	E_o	R12	P beam
ILC	0.6 mm	0.007	3.2 nC	3.03 MHz	1 TeV	16.4 m	1.24 kW
CLIC	0.4 mm	0.010	0.6 nC	2.00 GHz	3 TeV	25 m	288 kW

Table 4: Peak power in ILC and CLIC crab cavities.

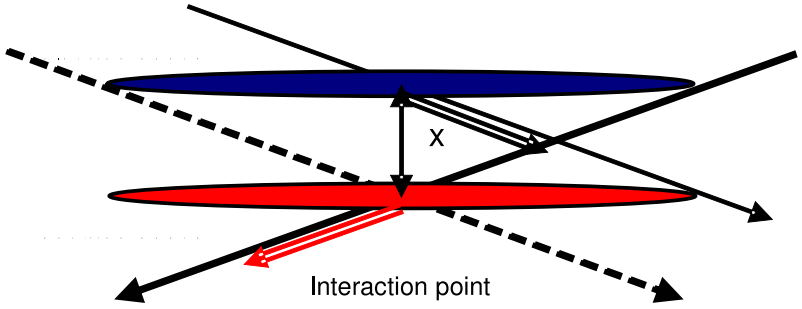

Figure 13: Crab cavity fields view.

missing by distance Δx as shown in Fig. 13 and for a horizontal beam size parameter σ_x is given as

$$S = \exp\left(-\frac{\Delta x^2}{4\sigma_x^2}\right) \tag{14}$$

Using Eq. (7) and expressing the timing error Δt as an angle one writes

$$\varphi = \omega \Delta t \tag{15}$$

where ω is the angular frequency of the RF. The luminosity reduction factor may therefore be written as

$$S(\varphi) = \exp\left\{-\left(\frac{c\,\theta_r\,\varphi}{2\,\sigma_x\omega}\right)^2\right\} \tag{16}$$

Were the phase errors have a Gaussian distribution then the RMS luminosity reduction factor is determined from

$$S_{\text{rms}}(\varphi_{\text{rms}}) = \sqrt{\frac{1}{\sqrt{2\pi}}\int_{-\infty}^{\infty}\frac{1}{\varphi_{\text{rms}}}\exp\left\{-2\left(\frac{c\,\theta_r\,\varphi}{2\,\sigma_x\omega}\right)^2\right\}\exp\left(-\frac{\varphi^2}{2\,\varphi_{\text{rms}}^2}\right)\,d\varphi} \tag{17}$$

hence

$$S_{\text{rms}}(\varphi_{\text{rms}}) = \left(1+\left(\frac{c\,\theta_r\varphi_{\text{rms}}}{\sigma_x\omega}\right)^2\right)^{-\frac{1}{4}} \tag{18}$$

	S	f (GHz)	σ_x (nm)	θ_c (rads)	ϕ_{rms} (deg)	Δt (fs)
CLIC	0.98	12.0	60	0.020	0.0251	6
CLIC (4 GHz)	0.98	4.0	60	0.020	0.0084	6
ILC	0.98	3.9	600	0.014	0.1164	83

Table 5: Phase tolerances for CLIC and ILC.

For small phase errors ϕ, $S_{\rm rms} \approx S$ and inverting this relation gives

$$\varphi_{\rm rms} = \frac{\sigma_x \omega}{c\theta_r}\sqrt{\frac{1}{S_{\rm rms}^4} - 1}\ \text{rad} \ = \frac{360\ \ \sigma_x f}{c\theta_r}\sqrt{\frac{1}{S_{\rm rms}^4} - 1}\ \text{degrees} \tag{19}$$

where $\phi_{\rm rms}$ is the acceptable phasing error of one cavity with respect to the other for a luminosity reduction factor $S_{\rm rms}$. The target limit on luminosity reduction from the crab system is about 0.98. Table 5 evaluates Eq. (19) for the CLIC at 12 GHz, CLIC at 4 GHz and the ILC as a comparison and also expresses the phase error as a timing error.

The phase control specification for the CLIC crab cavities is well beyond anything that has been demonstrated at the 100 kW input power level.

4.4 Technology Choice

The financial budget available for developing a crab cavity system guides the technology choice to one where power sources and major infra-structure are available at the collaborating laboratories. Whilst the use of a superconducting cavity or indeed a normal conduction cavity at 4 GHz is not ruled out, the future availability of high power klystrons at 12 GHz and infra-structure for the manufacture and testing of 12 GHz cavities leads us to the technology choice of 12 GHz copper structures for testing at CTF3 in 2012.

Given that beam loading is likely to be completely unpredictable for CLIC, our proposed solution is to have a power flow into and through the cavity that is significantly higher than the maximum beam loading power requirement. This is most easily realized with a high group velocity travelling wave cavity.

A reason for not favoring standing wave (SW) over travelling wave (TW) cavities is that measurement of phase in multi-cell cavities can have inaccuracies at the level of milli-degrees caused by the excitation of modes adjacent to the operating modes [15] and we expect these to be somewhat smaller for TW cavities. This is because the TW cavity will have lower Q factors and we expect that the phase shift when the cavity is not precisely on frequency will be distributed along the structure rather than being all across the input coupler as it would be for the SW cavity.

The proposal for synchronising the cavities is to use the scheme proposed for the NLC by J. Frisch where the output from a klystron is split and carried along equal lengths of temperature controlled waveguide to the crab cavities on opposing beams. With an advanced optical interferometer it may be possible to provide reference phases at the cavities that a synchronized to 1 fs [17]. The strategy is then to design a cavity which follows the input phase as closely as possible. To do this one might for instance mount the cavity centrally so that expansion gives

Phase advance per cell, φ radians	Length of the cell, D mm (11.994 GHz)
$2\pi/3$ (TW)	8.332
$5\pi/6$ (TW)	10.415
π (SW)	12.498

Table 7: Cell length for various phase advance choices.

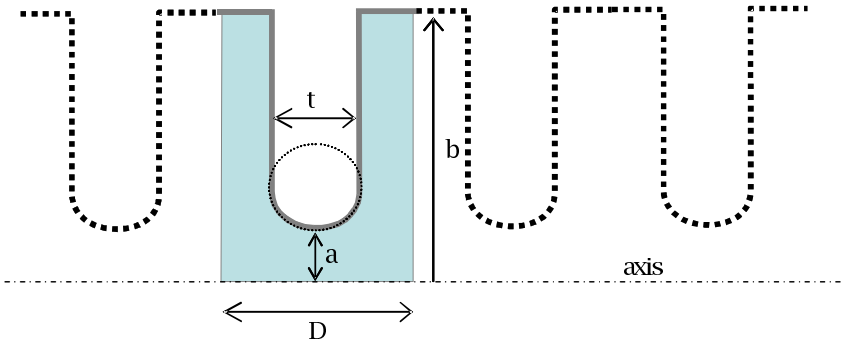

Figure 14: Crab cavity geometry.

phase errors that cancel. Careful attention to cavity temperature control will be needed so that the two systems perform in an identical fashion.

It is unlikely that cavity phase could ever be measured to an accuracy of milli-degrees and then corrected on the timescale of a few bunches (say 40 ns). If after actively matching waveguide paths to the input couplers it turns out that the relative phase of the two crab cavities drift with respect to each other during the pulse then the only possible correction scheme is to mix an RF power correction with the main split power using feed forward estimation from the previous bunch train.

The strategies for managing wakefields are large irises and strong damping.

4.5 Cavity Parameter Search

The first stage in the development of a cavity is to understand how key parameters such as group velocity, Q factor, R/Q and ratios of peak fields to fields on axis depend on dimensions. Figure 14 shows our choice of basic cell as part of an infinite structure with four variable parameters a, b, t and D. The iris curvature is circular with radius t/2. The properties are determined from field solutions with periodic boundary conditions. The cell length depends on the choice of phase advance per cell as give in Table 7.

Whilst the cell has four independent cell parameters one is fixed by frequency and one is fixed by phase advance hence investigative plots only vary iris thickness and iris radius. Figures 15 and 16 show parametric variations with iris radius and iris thickness, all curves correspond to a frequency of 11.994 GHz and the given phase advance is given in the sub figure header. Differing curves correspond to differing thicknesses. Note that a thickness of 8 mm almost consumes the entire cell.

In order to get a high group velocity Fig. 16 indicates that the $2\pi/3$ mode is a better choice than the $5\pi/6$ mode. As longitudinal space is not a major consideration we might also modes with wave numbers great than π such as consider the $4\pi/3$ mode. In order to control short range wakes to an acceptable we anticipate an iris radius approaching 5mm.

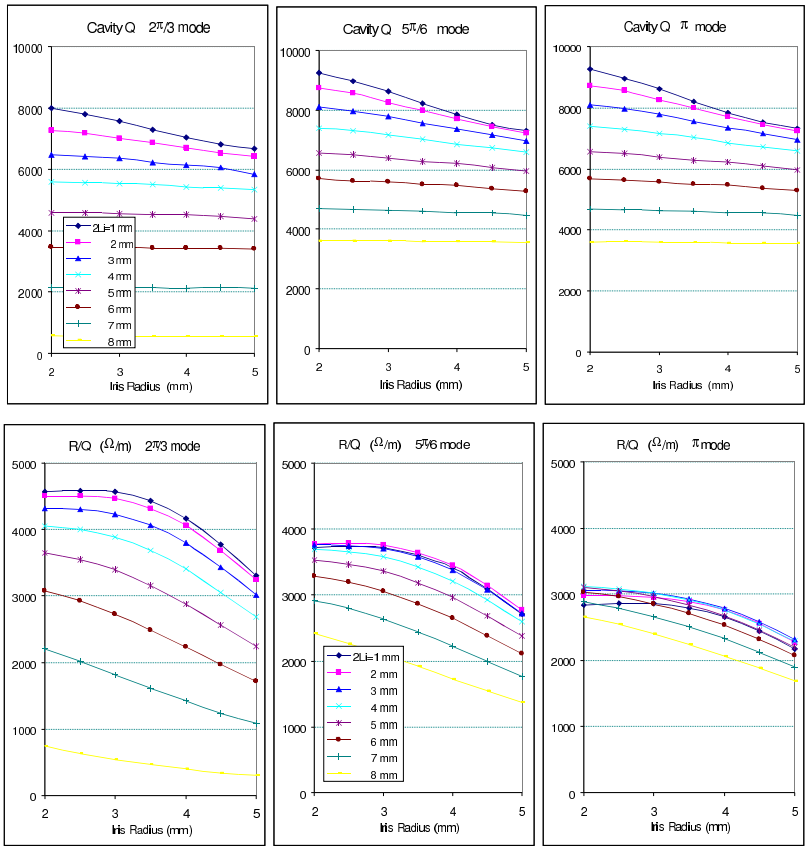

Figure 15: Parametric investigative plots varying iris radius and iris thickness.

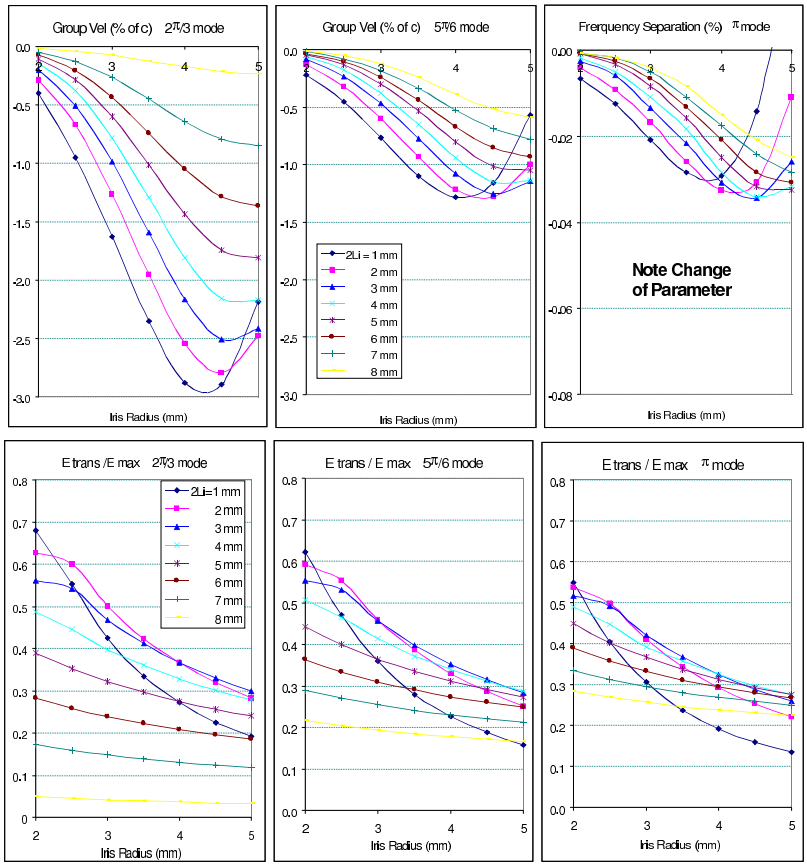

Figure 16: Parametric investigative plots varying iris radius and iris thickness.

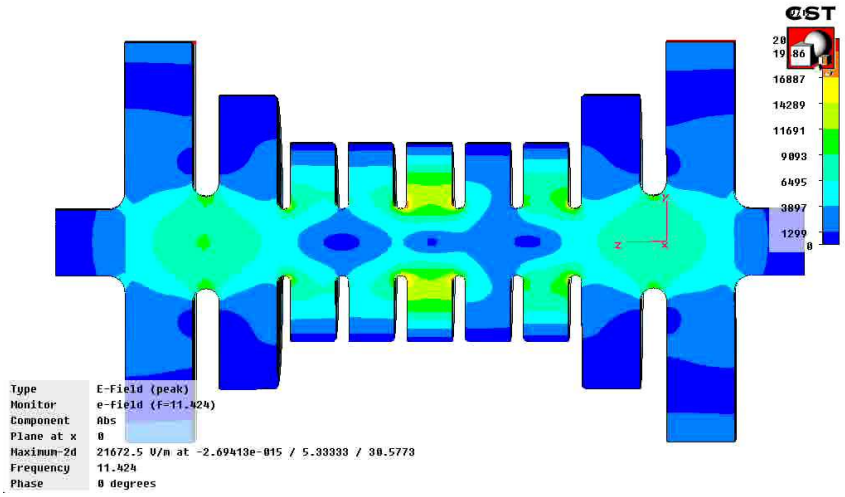

Figure 17: Peak electric field in the cavity with maximum gradient.

4.6 Gradient Testing

The absolute minimum number of cells for the CLIC crab cavity is determined by the maximum gradient. The maximum gradient for this type of cavity is unknown. The number of cells required for the CLIC cavity may need to be sufficient for wakefield de-coherence and this is under study. As heating effects are likely to upset phase stability, pushing to the minimum number of cells is unlikely to be the optimum solution unless wakefields are the determining factor. As the maximum gradient is an unknown, it makes sense to determine it for a typical manufacturing technology. This then sets a limit that one can work well beneath. A collaboration between SLAC and CI with hopefully make such a test possible. Figure 17 shows peak electric field in a cavity being designed to determine the maximum gradient. A key feature of this cavity is that the end cells are excited in a “TE111 like mode” so that the maximum gradient occurs in the centre cells which have “TM110 like excitation”.

A challenge with this type of this structure is impedance matching so that a pure forward travelling wave is obtained in the centre cells. Use of a procedure described by Alesini et al. [18] was attempted. This technique plots ratios of reflection coefficient for structures shorted at the n^{th} and $(n+1)^{th}$ cell centres as function of two matching cell parameters and then interpolates to find parameters giving the correct phase advance per cell with no attenuation. The technique did not seem to work very well for our cavity, possibly due to its asymmetry. A matching technique that did work for our cavity used a Floquet theorem approach [19].

4.7 Next Steps

- Investigate maximum gradient vs. pulse length for X-band dipole structure at SLAC
- Investigate pulse heating for dipole structures and its effect on phase stability.
- Develop damped structures.
- Cooling requirements and mechanical design.
- Determine likely phase and amplitude control performance for operation from a Klystron.
- Design beam test experiments.

5 CLIC Post-Collision Lines

Presenter: Konrad Elsener, CERN

5.1 A conceptual design

Due to the very large number of coherent pairs produced in a 3TeV collision, the CLIC post-collision line can not simply be a copy or extension of the ILC design. In ILC a beam energy and a beam polarisation measurement station are part of the beam diagnostics after the interaction point. For CLIC, a different approach has been proposed and is being pursued since a few years by A. Ferrari and colleagues [20, 21]. The main ingredients of the proposed scheme for CLIC are illustrated in Fig. 18. A set of four vertical bending magnets is used to separate lower energy particles from the beamstrahlung photons and from the main beam. Three sets of collimators are introduced in order to reduce particle losses in the magnets. An intermediate dump is designed to stop all the opposite-sign particles of the coherent pairs as well as the lower energy tail of same-sign particles. After this dump, a second set of vertical bending magnets is used to deflect the remaining beam back onto a horizontal trajectory. Beamstrahlung photons, the core of the beam as well as the remaining particles of energies above 250GeV are transported to a common dump (the water dump).

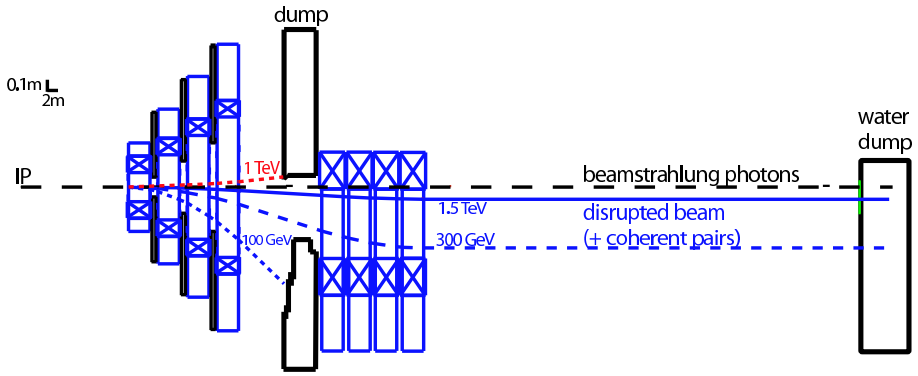

Figure 18: Conceptual design of the CLIC post-collision line (side view), as described in [21]. Same-sign particles from the IP are indicated in blue (300GeV dashed line, 1.5TeV solid line), opposite-sign particles in red (1 TeV dotted line). Note that this layout is drawn to scale, however the vertical and longitudinal scales differ by a factor 20. The overall length of the post-collision line is 160m.

5.2 Recent Evolution

A detailed look at the conceptual design of the post-collision line proposed in [21] reveals a number of issues:

- longitudinal space: elements are unrealistically close to each other
- lateral space: although the 20 mrad crossing angle rapidly provides beam separation in the horizontal plane, the space available is too small (e.g. 10cm between quadrupole of incoming beam and dipole of post-collision line)
- beam losses: the energy deposition by stray particles in some of the magnets appears too high.

As a remedy to some of these issues, variants of "stretched" versions of the post-collision line are being studied. Here, the distances between magnets are increased, and the field is lowered from 1T to 0.8T. As shown in Fig. 19, this does not impact on the overall layout (separation of particles), while the extra space allows for a more realistic design of components.

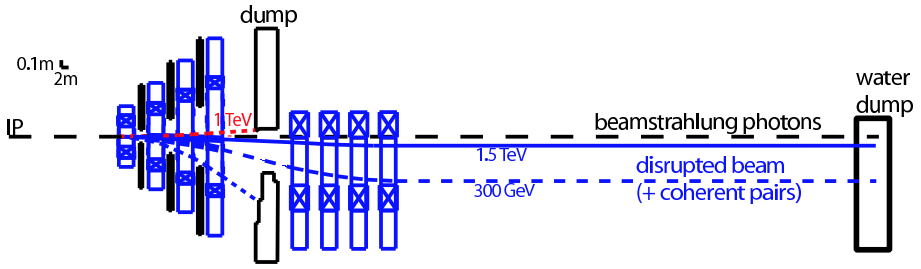

Figure 19: Proposal for a stretched version of the design proposed in [21]. The overall length of the post-collision line is increased to 240m.

At the time of CLIC08, work had started to address issues related to the particle losses in the first series of vertical deflection magnets. For example, an additional collimator before the first magnet had been introduced [22]. Additional intermediate dumps ("tail-clippers") were proposed to stop the 250-700 GeV particles - this would allow the water dump entrance window to have the dimension of the ILC design (diameter 30cm). Much work is still required to finalize all these aspects of the conceptual design. Some of the changes mentioned here are integrated into a report on an updated version of the post-collision design [23].

5.3 Beam Diagnostics in the Post-Collision Lines

Due to the large number of coherent pairs produced in collisions at CLIC, it will be difficult to use sophisticated beam diagnostics equipment in the post-collision lines. Several possibilities have been described in [25] and are summarized in [23]. One of the most crucial tasks to be performed in the post-collision line is luminosity-monitoring. Rather than measuring absolute values of the luminosity, the task is to provide a signal which can be used for re-tuning the beams, i.e. for re-optimising luminosity. Moreover, such a feedback must be provided as fast as possible (at least train-by-train, since a bunch-by-bunch feedback is probably impossible at CLIC). It has been shown [24] that the number of beamstrahlung photons is strongly correlated to luminosity. This implies that counting the number of such photons would be a valuable signal for luminosity monitoring. Two methods are currently envisaged for this task.

5.3.1 Muon pair-production by beamstrahlung photons

Beamstrahlung photons impinging on the water dump will predominantly produce electron pairs and thus e.m. showers. A substantial fraction of these very high energy photons will, however, produce muon pairs. While the e.m. showers are fully absorbed in the dump, the high energy muons will penetrate the exit wall of the beam dump cavern. As proposed in [25], these muons can be observed with a gas-filled Cerenkov counter, using a photomultiplier. First estimates show that one can expect about 4×10^5 Cerenkov photons per bunch. Using the Cerenkov technique allows, moreover, being sensitive to the direction of the muons, thus efficiently suppressing background muons produced in the beam delivery system of the incoming beam which passes at a few meters lateral distance only.

5.3.2 Electron pair-production by beamstrahlung photons

A second way of counting beamstrahlung photons has been proposed [26]. The photons would be converted into electron pairs in a thin carbon disc, located half-way between the last magnet of the post-collision line and the water dump. The electron pairs could be observed via the optical transition radiation they produce when traversing in a thin foil. This OTR technique

is widely used for beam observation at high energy accelerators. Out of the 2.5×10^{12} beamstrahlung photons in a 156ns pulse train at CLIC, a 1mm thick carbon converter would produce 5×10^{9} charged particles, which can rather easily be observed using the OTR method. A weak magnetic field between carbon converter and OTR screen would be sufficient to remove low energy electrons such as those produced from synchrotron radiation. Other sources creating background at the proposed detector location still need to be investigated.

5.3.3 The request for a Compton polarimeter in the CLIC post-collision line

One of the results of CLIC08, concerning the post-collision line, is the explicit request by the physics community to provide a measurement of the beam polarisation after the interaction point. This is discussed in some detail by K. Moffeit, in section 13 of this note.

PLACET:	rms [nm]	σ_y [nm]
zero energy spread		
w/o ISR	0.88	0.81
w ISR	1.83	0.96
1% linear energy spread		
w/o ISR	1.04	0.83
w ISR	2.48	1.00
0.4% Gaussian energy spread		
w/o ISR	1.36	0.89
w ISR	2.41	1.07
DIMAD	rms [nm]	
0.4% Gaussian energy spread		
w/o ISR	1.35	
w ISR	2.52	

Table 8: RMS and σ coming from a gaussian fit of the vertical IP beam sizes. The beam sizes with and without Incoherent Synchrotron Radiation (ISR) in the CLIC BDS, for different beam energy spread are evaluated with PLACET. DIMAD rms values are shown for comparison.

6 Incoherent synchrotron radiation studies

Presenters: Deepa Angal-Kalinin, CI, and Barbara Dalena, CERN

The emission of synchrotron radiation in the CLIC BDS results in an increase of the beam emittance (and as a consequence of the IP beam spot size), due to the incoherent energy spread generated by the quantized radiation emitted by the bended high energy beam. In addition, if the energy spread of the incoming beam is large the full compensation of the chromaticity cannot be achieved, this results in an increase of the IP spot size too. Therefore Incoherent Synchrotron Radiation gives a limit in the maximum luminosity achievable by limiting the minimum beam spot size at IP.

Tracking the beam throught the CLIC BDS with PLACET [27] we have evaluated the expected vertical rms and σ of the beam at IP, with and without incoherent synchrotron radiation emission. Table 8 shows these values for zero energy spread, 1% linear energy spread and 0.4% gaussian energy spread, rms values from DIMAD [28] for 0.4% Gaussian energy spread are also reported.

Fig. 20 shows the study of the emittance growth due to incoherent synchrotron radiation in CLIC BDS (top) with the BETA [29] code, about 25% emittance growth is expected for CLIC BDS while the same study for ILC (bottom) gives an emittance growth of 0.4%. Comparable result comes from the evaluation of the relative luminosity loss by running GUINEA-PIG when synchrotron radiation in all the CLIC BDS is taken into account.

The relative peak luminosity loss due to incoherent synchrotron radiation is reported in Table 9. By switching on and off the synchrotron radiation in the different type of elements of the CLIC BDS (i.e. quadrupole, bending magnet and multipole). It has been found that about 10% of the luminosity loss is due to bending magnet in the final focus and about 10% comes from the last quadrupole (QD0). The luminosity loss due to the final quadrupole is mainly due to

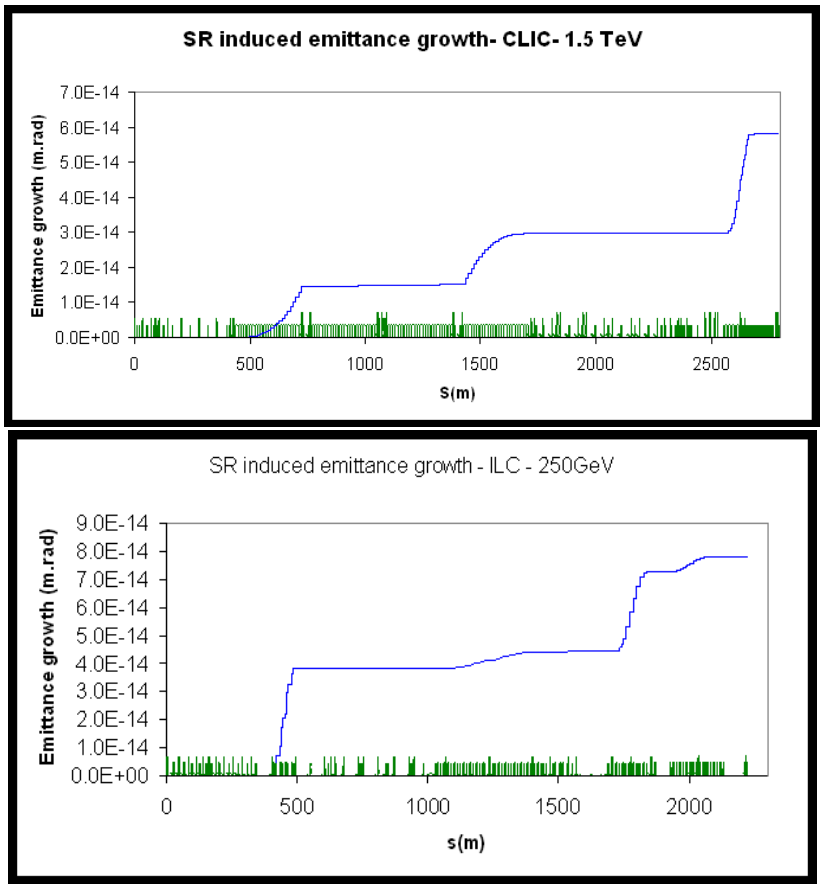

Figure 20: Emittance growth due to Incoherent Synchrotron Radiation in the CLIC BDS at 1.5 TeV. The ILC case at 250 GeV is shown too.

	peak lumi ($\times 10^{34}$m^{-2})	L/L$_0$
ALL ISR OFF	2.22 ± 0.03	1.00 ± 0.02
All ISR ON	1.72 ± 0.05	0.78 ± 0.02
ISR QUAD ON only	2.00 ± 0.03	0.90 ± 0.02
ISR MULTI ON only	2.22 ± 0.04	1.00 ± 0.02
ISR SBEND ON only	1.92 ± 0.02	0.86 ± 0.02
ISR QD0 OFF only	1.91 ± 0.02	0.87 ± 0.02
ISR QD0 ON only	2.00 ± 0.03	0.90 ± 0.02

Table 9: Luminosity in the peak and relative luminosity loss due to Incoherent Synchrotron Radiation. Peak luminosity and relative luminosity loss due to the Incoherent Synchrotron Radiation in the different type of elements of the CLIC BDS are shown too.

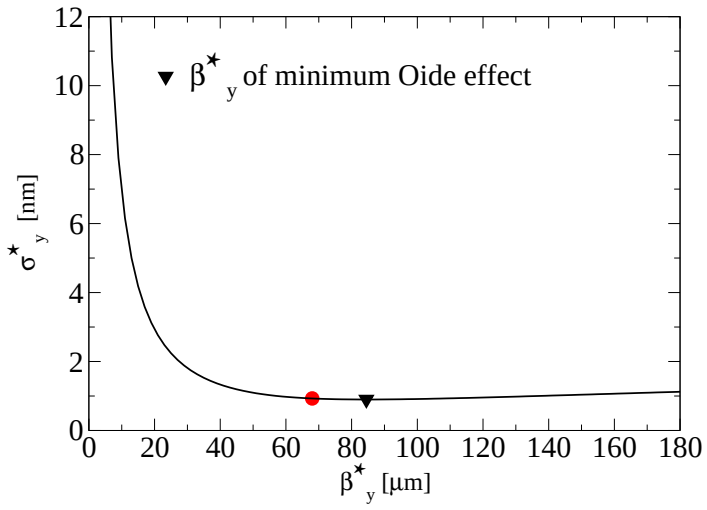

Figure 21: Vertical beam size as a function of the beta function at the collision point. The solid line is obtained from Eq.(11) of Ref. [30]. The red circle represent the calculated CLIC beta function at IP for 1.5 TeV. The beta function corresponding to the minimum Oide Effect (triangle) for the nominal CLIC normalized vertical emittance (20 nm rad) is also shown.

the incoming beam energy spread while the Oide Effect plays a minor role, as shown in fig. 21.

7 Computation of Resistive Wakefields

Presenter: Roger Barlow, University of Manchester

The Longitudinal $m = 0$ resistive wakefield has been studied in the long range approximation by Chao [31] and at short range with some other approximations by Bane and Sands [32] We show how it can be evaluated without these approximations. We go on to evaluate Longitudinal $m > 0$ wakefields and Transverse wakefields. We consider a frequency-dependent complex AC conductivity, and the implementation of this method in simulation codes being used for particle tracking simulations in CLIC.

We assume a uniform circular pipe of radius b, conductivity σ and match the solutions of Maxwell's equations in vacuum and in the (thick) metal pipe. These can be decomposed into angular modes ($cos(m\theta), m = 0, 1, 2...$). This is done in frequency space as differentiation $\rightarrow$ multiplication

7.1 The longitudinal wake for m=0

The Fourier Transformed wake is given by Chao:

$$\tilde{E}_z(k) = \frac{2q}{b}\frac{1}{\frac{ikb}{2} - \left(\frac{\lambda}{k} + \frac{k}{\lambda}\right)\left(1 + \frac{i}{2\lambda b}\right)}$$

where

$$\lambda(k) = \sqrt{\frac{2\pi\sigma|k|}{c}}(i + sgn(k))$$

Introduce s_0, the *scaling length* (20μ for 1 cm Copper)

$$s_0 = \sqrt[3]{\frac{cb^2}{2\pi\sigma}} \qquad K = s_0 k \qquad s' = \frac{s}{s_0}$$

The Wake is a function of three parameters (s, b and σ), but use of s_0 enables it (for the simpler approximations) to be written as a universal function $f(s')$, where $E_z(s, b) = \frac{q}{b^2} f(s/s_0)$.

7.1.1 The long range case

In the long range limit

$$\tilde{E}_z = -\frac{2qk}{\lambda b}$$

the Fourier Transform is well known to be

$$E_z(s) = \frac{q}{2\pi b}\sqrt{\frac{c}{\sigma}}s^{-\frac{3}{2}}$$

. We evaluate it the hard way by numerical integration of:

$$E_z(s) = \frac{1}{s_0\pi}\int_0^\infty \Big(Re[f_{even}(K)]\cos(Ks') + Im[f_{odd}(K)]\sin(Ks')\Big)dK$$

where

$$f_{even} = \frac{1}{2}\Big[f(K) + f(-K)\Big] = -\frac{q}{b^2}\sqrt{K} \quad f_{odd} = \frac{1}{2}\Big[f(K) - f(-K)\Big] = i\frac{q}{b^2}\sqrt{K}$$

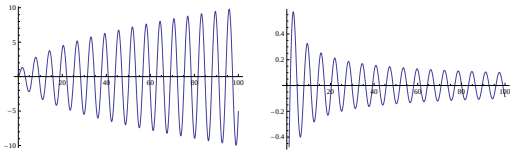

Figure 22: Oscillatory functions

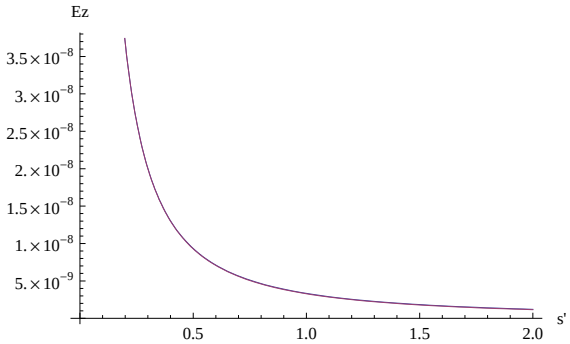

Figure 23: The long range wake

$\sqrt{K}sinKx$ oscillations increase so numerical integration $\int_0^\infty dK$ appears hopeless. However by first integrating analytically wrt x the function becomes $-cos(Kx)/\sqrt{K}$. The numerical integration wrt K is then possible - the oscillations get smaller as $K \to \infty$. Then one can differentiate numerically wrt x

Figure 23 shows our results and the Chao formula superimposed.

7.1.2 A more accurate formula

The next approximation is

$$\tilde{E}_z = \frac{2q}{b}\frac{1}{\frac{ikb}{2} - \frac{\lambda}{k}}$$

the solution of which was given by Bane and Sands

$$E_z(s) = \frac{4qc}{\pi b^2}\left(\frac{e^{-s'}}{3}cos(\sqrt{3}s') - \frac{\sqrt{2}}{\pi}\int_0^\infty \frac{x^2 e^{-x^2 s'}}{x^6+8}dx\right)$$

We can again separate and integrate numerically

$$f_{even}(K) = -\frac{q}{b^2}\frac{\frac{2}{\sqrt{K}}}{\left(\frac{K}{2} - \frac{1}{\sqrt{K}}\right)^2 + \frac{1}{K}}, f_{odd}(K) = -\frac{q}{b^2}\frac{2i\left(\frac{K}{2} - \frac{1}{\sqrt{K}}\right)}{\left(\frac{K}{2} - \frac{1}{\sqrt{K}}\right)^2 + \frac{1}{K}}$$

Figure 24 shows our results for both this approximation and the long range one. The analytical results of Bane and Sands are reproduced.

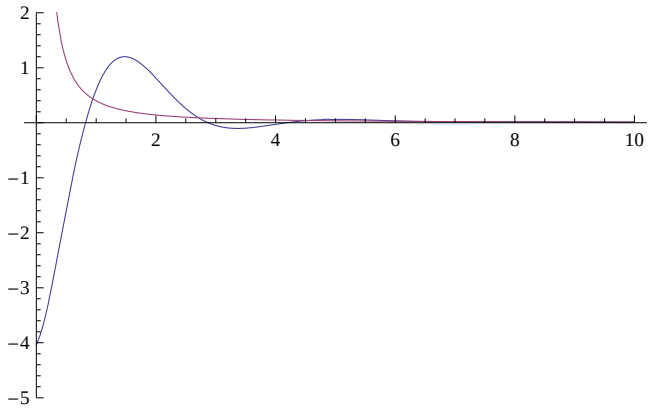

Figure 24: Long range and short range approximations.

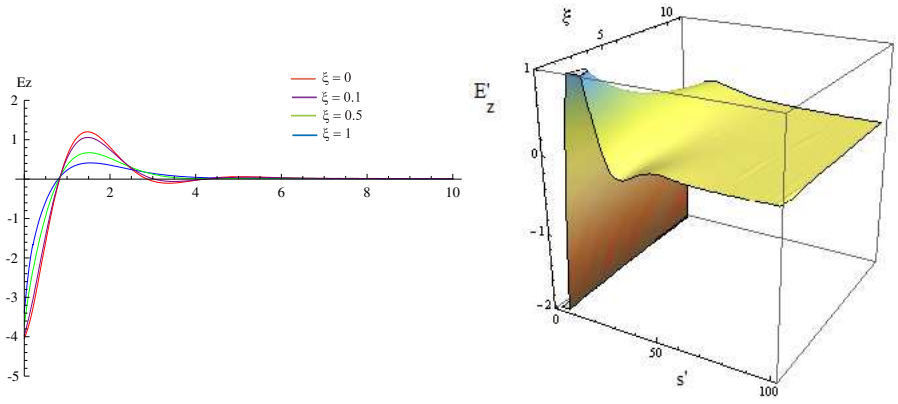

Figure 25: The wake as a function of s' and ξ

7.1.3 The full formula

Having validated our method usng the approximate solutions, we now apply it to the full version of the basic formula:

$$f_{even}(K) = -\frac{8q}{b^2}\frac{\xi^2 + \xi 2\sqrt{K} + 4\frac{\sqrt{K}}{K}}{4\left[\xi\sqrt{K} - \frac{1}{K}\left(\xi + 2\sqrt{K}\right) + K\right]^2 + \left(\xi^2 + \xi 2\sqrt{K} + 4\frac{\sqrt{K}}{K}\right)^2}$$

$$f_{odd}(K) = -\frac{8iq}{b^2}\frac{2\left[\xi\sqrt{K} - \frac{1}{K}\left(\xi + 2\sqrt{K}\right) + K\right]}{4\left[\xi\sqrt{K} - \frac{1}{K}\left(\xi + 2\sqrt{K}\right) + K\right]^2 + \left(\xi^2 + \xi 2\sqrt{K} + 4\frac{\sqrt{K}}{K}\right)^2}$$

with $\xi = s_0^2/b^2$. Although no longer a universal curve, this can still be expressed as a function of two variables (s' and ξ) rather than the full set of three. Bane and Sands' approximation corresponds to $\xi = 0$. Figure 25 shows how the function changes for different values of ξ. For ξ below about 0.1 the approximation is very good. (For a copper beam pipe with a radius of 1 cm $\xi \approx 0.000004$.)

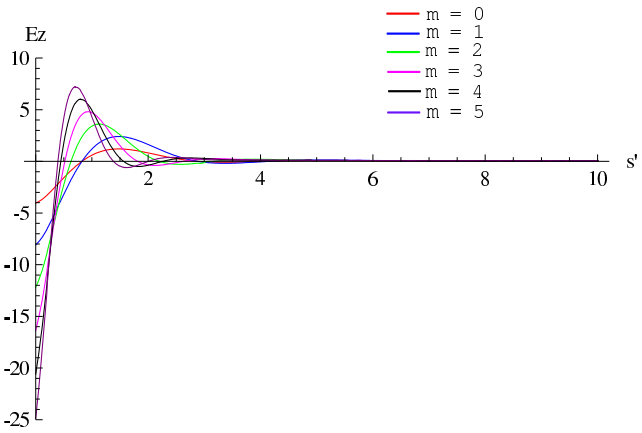

Figure 26: Higher order longitudinal modes in the Bane and Sands' approximation

7.2 Longitudinal wakes: Higher order modes

For higher modes, using the same technique gives

$$\tilde{E}_z^m = \frac{4}{b^{2m+1}} \frac{1}{\frac{\imath kb}{m+1} - \left(\frac{2k}{\lambda} + \frac{\lambda}{k}\right)\left(1 + \frac{\imath}{2\lambda b}\right) - \frac{\imath m}{kb}}$$

The equivalent of Bane and Sands' approximation is

$$\tilde{E}_z^m = \frac{4}{b^{2m+1}} \frac{1}{\frac{\imath kb}{m+1} - \frac{\lambda}{k}}$$

This can be separated into odd and even parts, and integrated numerically as before. Figure 26 shows results for $m = 0$ to $m = 5$.

The full formula can be separated into odd and even parts and integrated just as easily. Figure 26 shows the dependence on ξ for the $m = 1$ and $m = 5$ modes as examples.

$$f_{even}(K) = -\frac{8}{b^{2m+2}} \frac{\xi^2 + \xi 2\sqrt{K} + 2\frac{\sqrt{K}}{K}}{\left[\xi 2\sqrt{K} - \frac{1}{K}(\xi + 2\sqrt{K}) + 2\left(\frac{K}{m+1} - \xi\frac{m}{K}\right)\right]^2 + \left(\xi^2 + \xi 2\sqrt{K} + 2\frac{\sqrt{K}}{K}\right)^2}$$

$$f_{odd}(K) = -\frac{8i}{b^{2m+2}} \frac{\left[\xi 2\sqrt{K} - \frac{1}{K}(\xi + 2\sqrt{K}) + 2\left(\frac{K}{m+1} - \xi\frac{m}{K}\right)\right]}{\left[\xi 2\sqrt{K} - \frac{1}{K}(\xi + 2\sqrt{K}) + 2\left(\frac{K}{m+1} - \xi\frac{m}{K}\right)\right]^2 + \left(\xi^2 + \xi 2\sqrt{K} + 2\frac{\sqrt{K}}{K}\right)^2}$$

The dependence on ξ increases for higher modes but still looks ignorable for any sensible collimator, see Fig. 27.

7.3 Transverse wakes

The transverse wake is also a sum over angular modes

$$\vec{E_T}(r, \theta, s) = \sum_m r^{m-1} r'^m (\hat{r} cos(m\theta) - \hat{\theta} sin(m\theta)) W_T^m(s)$$

The Panofsky-Wenzel theorem applies term by term giving $W_T^m(s) = \int_0^s E_z(x)dx$. Luckily we have already evaluated that integral already as the means of integrating the increasing oscillations in the longitudinal wake. So transverse wakes can be calculated for any order, in the full formula or with approximations. Figure 28 shows the wakes for various modes with $\xi = 0$.

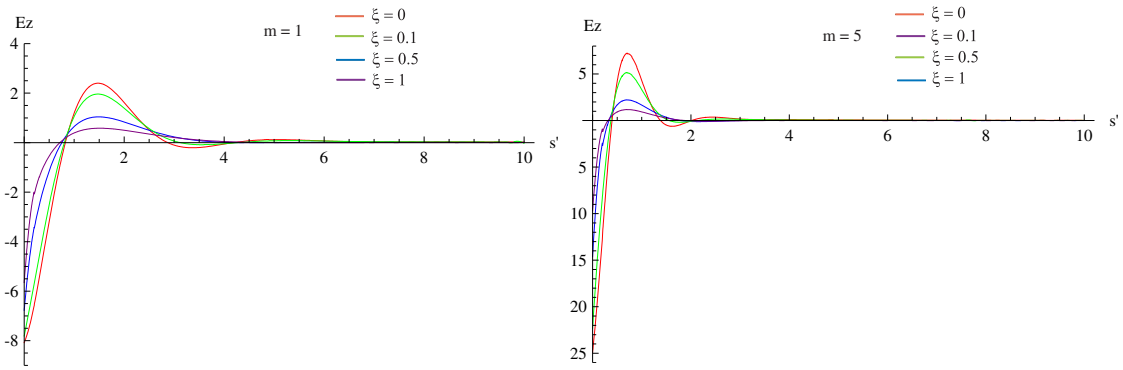

Figure 27: $m = 1$ and $m = 5$ longitudinal wakes for some values of ξ

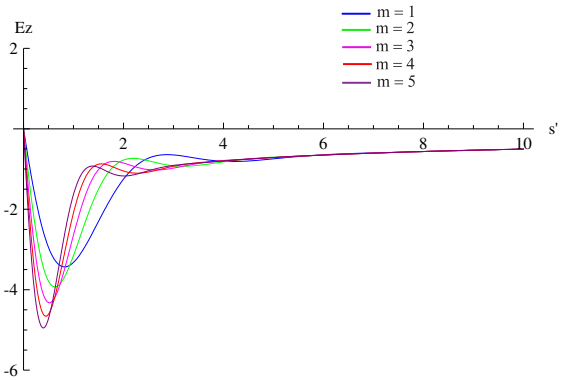

Figure 28: Transverse wakes - various modes with ξ=0

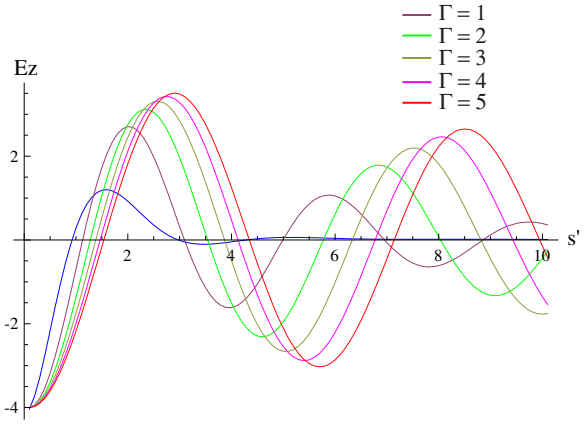

Figure 29: The $m = 0$ wake for various Γ

7.4 AC conductivity

In the Drude model for electrons in a conductor the conductivity is not a constant but includes a frequency/wavelength dependent imaginary part. It can be written $\tilde{\sigma} = \frac{\sigma}{1 - ikc\tau} = \frac{\sigma}{1 - iK\Gamma}$ where Γ typically of order 1 at most. We introduce into previous formulae and proceed as before. The wakes are now also a function of Γ. Figure 29 shows that nonzero values of Γ increase the size and the range of the wake effects.

7.5 Implementation

We use Mathematica[33] to integrate even and odd functions and generate tables of values as function of s', ξ, Γ which are written to files, available from the authors [34]. There are separate files for tranverse and longitudinal wakes, and for order up to $m = 5$ (currently). ξ and Γ do not vary for a given collimator. so we have written a portable `C++` object `collimatortable(file,Gamma,xi)` which reads complete 3-D table and interpolates to get single table for s'. `double collimatortable::interpolate(double x)` then returns the value of the wake for this collimator at the desired separation.

Implementation in MERLIN is straightforward as it fits into the existing structure[35]. Class `ResistivePotentials` inherits from `SpoilerWakePotentials` It reads the tables when created and contains functions `Wtrans(z,m)` and `Wlong(z,m)` which each return a value from the tables (using parabolic interpolation), scaled by appropriate factors.

PLACET currently includes only the $m = 1$ transverse mode though (unlike MERLIN) it does include rectangular collimators through the Yokoya Ansatz $y_{trailing} \rightarrow 0.822 \times y_{trailing} + 0.411 \times y_{leading}$ We have implemented it using the `collimatortable` object.

7.6 Examples

MERLIN has been used to evaluate resistive contributions to kick factors for ESA test collimators[36]. It shows that they are much less than geometric wakes (and than the measurement errors). Figure 30 shows the results of a PLACET simulation. The leading particles (on the left of the plot) receive no kick: for later particles the kick is greater.

7.7 Future developments

This technique can be used to study resistive wake effects using particle trcing codes for full lattices isuch as those for CLIC, the ILC and the LHC. The approach will be extended to

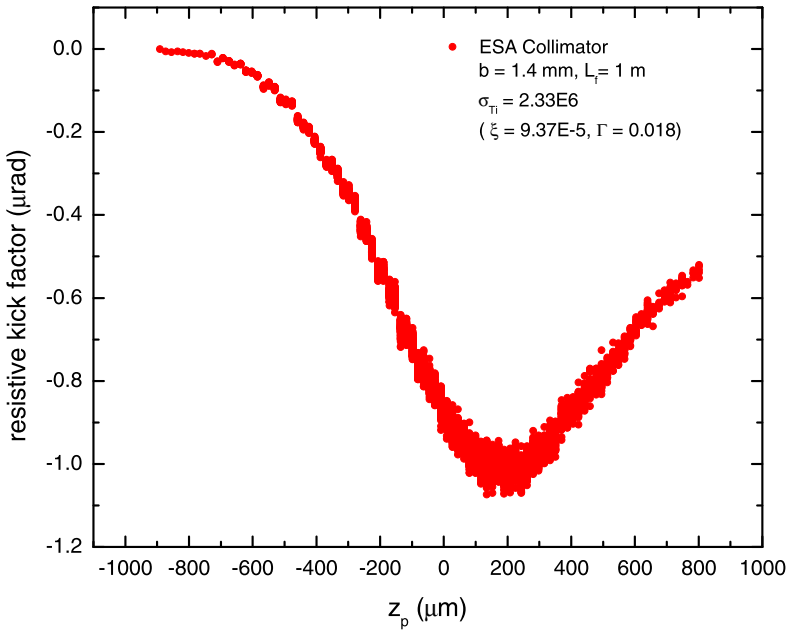

Figure 30: Kicks on individual particles in a bunch

rectangular apertures shortly.

8 Halo and Tail generation study at low energy

Presenter: Ijaz Ahmed, CERN

The CLIC test facility will demonstrate the essential parts of the CLIC drive beam generation scheme consisting of a fully loaded linac, a delay loop and a combiner ring [37]. The final CTF3 drive beam delivered to the CLIC Experimental Area (CLEX) comprising the test beam line and a two beam test stand, has an energy of 150 MeV, 35 A of beam current, a bunch repetition frequency of 15 GHz and a pulse length of 140 ns. Main differences between the CTF3 beam and the CLIC drive beam are the energy and the current. The CLIC drive beam has a beam current of 180 A and is decelerated from 2.397 GeV to 0.23 GeV giving up 90% of its energy. The aim of TBL is to extract as much energy as possible out of the beam and to demonstrate the stability of the decelerated beam and the produced rf power. The main issues are the transport of a beam with a very high energy spread with no significant beam loss and suppression of the wake fields from the power extraction and transfer structures (PETS). Finally TBL will produce RF power in the GW range which could be used to test several accelerating structures in parallel. Since last decade the increasing interest for high-intensity, high-energy linear accelerators have induced the scientific community to consider a phenomenon whose effects are worrying: the beam losses. Lost particles can, indeed, produce complicated problems in operation and maintenance of the machine. Usually such kind of particles originate in a low-density particles called halo which can extend far from the beam core and are small fraction of beam particles. Analytical estimates are undertaken in order to understand the physics of halo production and to develop methods to limit and control beam losses. The present work reviews efforts and advances in beam-halo. The previous study was performed mainly for high energy beam for beam delivery system for linear colliders. We have now studied and extended these simulations to lower energies as relevant for the CLIC drive beam.

We describe the main processes which contribute among the halo generation with analytic estimates and with preliminary simulations in the CTF3 Test Beam Line (TBL) and CLIC drive beam. We calculate and simulate particle scattering and radiation processes. When core particles significantly increase in amplitude, they become halo particles. Mainly the contributing process for the production of halo is:

- Beam Gas elastic scattering (Mott)
- Beam Gas inelastic scattering (Bremsstrahlung)

The Monte Carlo halo generator code for the particle scattering processes is provided by the package called HTGEN. The previously, studies for halo and tail generation study were performed for ILC [38] and for CLIC beam delivery system [39]. An analytical estimate for elastic beam-gas scattering is calculated for a constant normalized emittance of 150μrad at β_y=3.40164m. ρ is the density of nitrogen gas molecules per cubic meter and P the scattering probability per electron per meter over the CTF3-TBL we find that an electron has a probability of about 3.37×10^{-10} to undergo elastic scattering with an angle of at least the beam divergence equal to 329 μrad. The probability integrated over the CTF3-TBL is about 7.41×10^{-9}. As probability integrated over the CLIC drive beam we get about 1.202×10^{-6}. The probability for inelastic scattering with a fractional energy loss Kmin > 0.01, is 1.77×10^{-13}m in the CTF3-TBL and rather similar in the CLIC Drive beam. In the simulation, the beam gas temperature, pressure and other parameters are shown in table 10.

The simulations described here were performed for an ideal machine without errors and positioning tolerances. For the nominal intensity of 1.4575Œ 1010 particles per bunch and 200 bunches in TBL, we expect that 2.16×10^{4} particles are scattered and named as halo particles, in each train crossing. Similarly for the case of CLIC drive beam, with particle intensity of

CTF3-TBL LENGTH [m]	21.99
CLIC Drive Beam Length [m]	738.349
Z mean (N2)	7
Pressure [nTorr]	10
Temperature [K]	300
Npart	4×10^9
Kmin	0.01
Particle density [$10^{14}m^{-3}$]	6.438

Table 10: CLIC and CTF3 parameters

Location	E [GeV]	Gas	σ_{el} [barn]	σ_{in} [barn]	P_{el} [m^{-1}]	P_{in} [m^{-1}]	θ_{min} [μrad]
CTF3-TBL	0.150	N_2	5242	5.5117	3.37×10^{-10}	1.77×10^{-13}	329
CLIC DB	2.397	N_2	25146.2	5.5117	1.628×10^{-9}	1.77×10^{-13}	9.4

Table 11: Parameters for the CTF3 and CLIC halo generation.

5.25×10^{10} per bunch and 50 bunches in train will produce 3.15×10^{6} halo per train.

Figures 31 and 32 show the deceleration of the halo particles through the CLIC drive beam and TBL after passing through successive decelerating structures. The tracking has been performed by a detailed tracking package PLACET [47], with relevant parameters in 11.The decelerating structures are assumed to have one longitudinal and one transverse mode. Each of these two modes can be described by a loss factor, a wavelength, a group velocity and a damping. The PETS model includes single and multi bunch effect. The monopole field is used to decelerate while the set of dipole modes gives kick on the transverse plane.

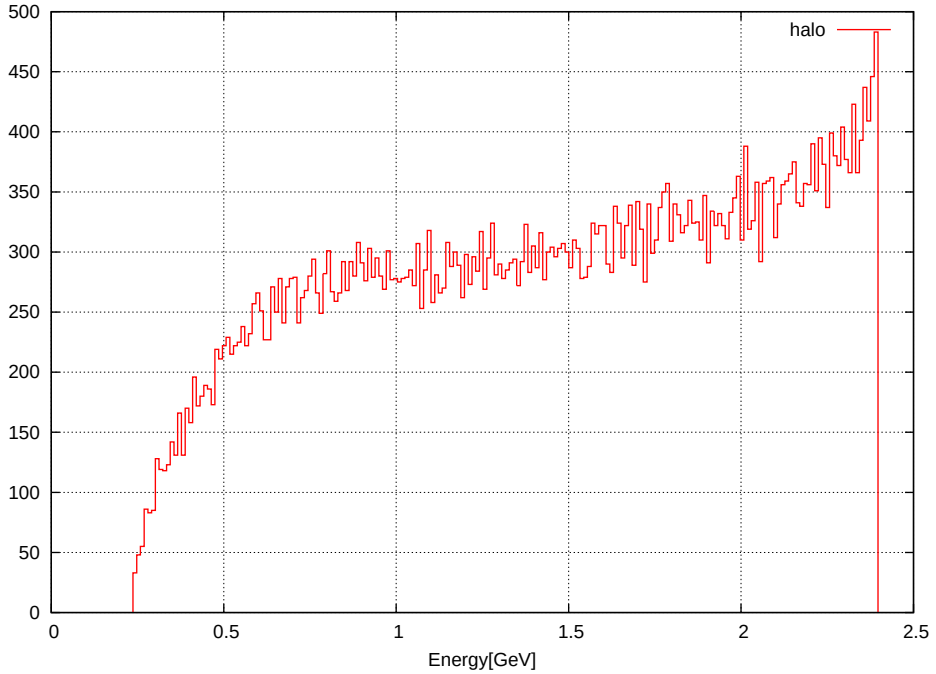

Figure 31: Energy of the Halo particles at the end of the CLIC drive beam.

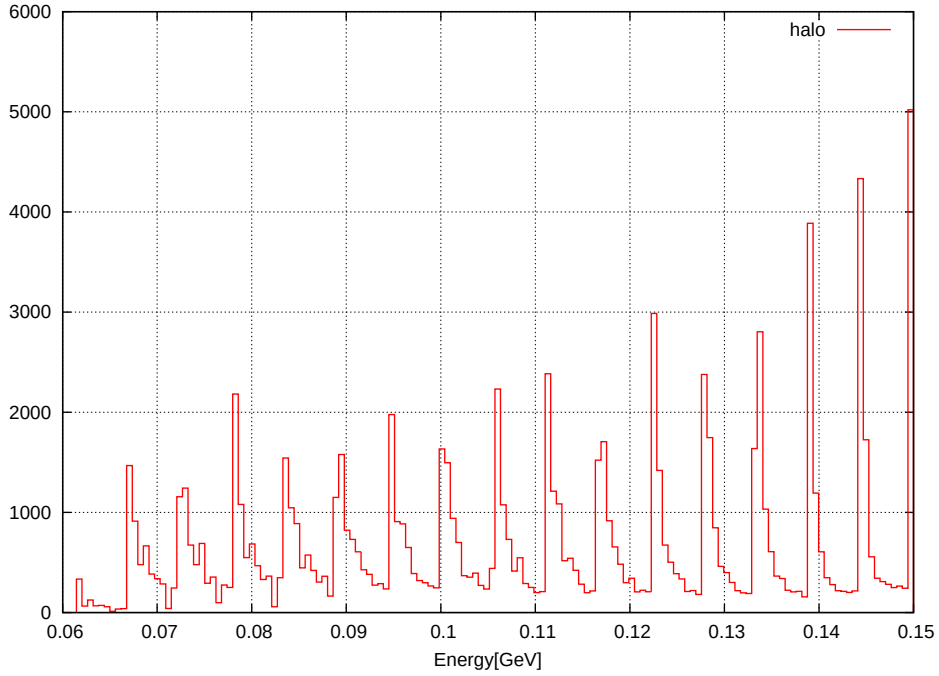

Figure 32: Energy of the Halo particles at the end of the CTF3 TBL drive beam.

9 CLIC collimation system review

Presenter: Javier Resta Lopez, Oxford

9.1 Introduction

The CLIC beam parameters have recently been optimised [10] and the optics of the Beam Delivery System (BDS) has accordingly been modified [2]. However no significant changes

have been done to the optics of the collimation section (see Fig. 33).

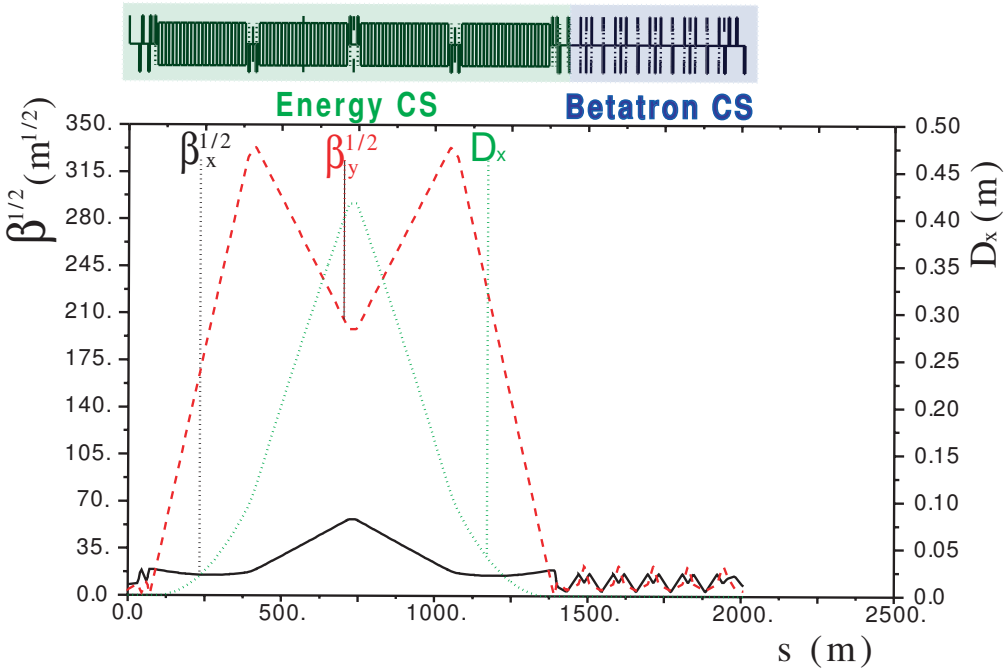

Figure 33: Horizontal dispersion and square root of the betatron functions for the CLIC baseline collimation system.

The first postlinac collimation section is dedicated to energy collimation. The energy collimation depth is determined by failure modes in the linac [40]. A scheme spoiler/absorber, located in a region with non-zero horizontal dispersion, is used for intercepting mis-steered or errant beams with energy deviation larger than about $1.3\ \%$ of the nominal energy.

Downstream of the energy collimation section, a dispersion-free section, containing eight spoilers and eight absorbers, is dedicated to the cleaning of the transverse halo of the beam, reducing thus the experimental background in the Interaction Point (IP). For linear colliders, the necessary betatron collimation depths are typically determined from the condition that beam particles and synchrotron radiation photons emitted in the final quadrupoles should not hit any magnet apertures on the incoming side of the IP. According to this criterium, first order estimate of collimator gaps using synchrotron radiation ray tracing through the interaction region has determined the following collimation depths: $16\ \sigma_x$ (horizontal) and $70\ \sigma_y$ (vertical) [41]. Since this estimate is based on linear transport and the nonlinear effects seem to be very strong in the CLIC final focus, a safer criterium is simply the protection of the final quadrupole QD0 against particle hitting, i.e. the bore aperture of QD0 determines the actual betatron collimation depth: $10\ \sigma_x$ (horizontal) and $44\ \sigma_y$ (vertical) [42]. Table 12 summarises the CLIC post-linac collimator parameters. The horizontal aperture for the momentum collimator is set to $a_x = D_x\delta_{\rm aper}$, with the energy offset $\delta_{\rm aper} = \pm 1.3\ \%$.

9.2 Spoiler Survivability

The energy spoiler has been designed with the condition of surviving in case of a deep impact of an entire bunch train or, at least, withstanding the impact of as many bunches as possible.

Earlier studies [43] concluded that a spoiler made of beryllium (Be) might be a suitable solution in terms of high robustness and acceptable wakefields.

Table 12: CLIC post-linac collimator parameters. Longitudinal position, horizontal and vertical β-functions, horizontal dispersion, horizontal and vertical half gaps, geometry of the collimator and material.

s[m]	Name	β_x[m]	β_y[m]	D_x[m]	a_x[mm]	a_y[mm]	Geometry	Material
907.098	ENGYSP	1406.33	70681.9	0.27	3.51	25.4	rect	Be
1072.098	ENGYAB	3213.03	39271.5	0.417	5.41	25.4	rect	Ti(Cu coated)
1830.872	YSP1	114.054	483.253	0.	10.	0.08	rect	Be
1846.694	XSP1	270.003	101.347	0.	0.08	10.	rect	Be
1923.893	XAB1	270.102	80.9043	0.	1.	1.	ellip	Ti(Cu coated)
1941.715	YAB1	114.054	483.184	0.	1.	1.	ellip	Ti(Cu coated)
1943.715	YSP2	114.054	483.188	0.	10.	0.08	rect	Be
1959.537	XSP2	270.002	101.361	0.	0.08	10.	rect	Be
2036.736	XAB2	270.105	80.9448	0.	1.	1.	ellip	Ti(Cu coated)
2054.558	YAB2	114.055	483.257	0.	1.	1.	ellip	Ti(Cu coated)
2056.558	YSP3	114.054	483.253	0.	10.	0.08	rect	Be
2072.379	XSP3	270.003	101.347	0.	0.08	10.	rect	Be
2149.579	XAB3	270.102	80.9043	0.	1.	1.	ellip	Ti(Cu coated)
2167.401	YAB3	114.054	483.184	0.	1.	1.	ellip	Ti(Cu coated)
2169.401	YSP4	114.054	483.188	0.	10.	0.08	rect	Be
2185.222	XSP4	270.002	101.361	0.	0.08	10.	rect	Be
2262.421	XAB4	270.105	80.9448	0.	1.	1.	ellip	Ti(Cu coated)
2280.243	YAB4	114.055	483.257	0.	1.	1.	ellip	Ti(Cu coated)

Recently we have revisited the spoiler heating issue considering the new beam parameters [44]. For example, the new vertical normalised emittance is $\gamma\epsilon_y = 20$ rad·nm (previously it was $\gamma\epsilon_y = 10$ rad·nm), and the current bunch train intensity is 312 bunches $\times\ 3.72 \times 10^9$ particles/bunch (2008 parameters), which is approximately twice than the old value 220 bunches $\times$ 2.56×10^9 particles/bunch (2005 parameters).

The principal mechanism for spoiler damage is the instantaneous heat deposition . The main sources for such a heating are the energy deposition by direct beam-spoiler impact, the image current heat deposition (ohmic heating) and electric field breakdown. Assuming a thin spoiler ($\approx 0.5\ X_0$, with X_0 the radiation length of the material), in case of a deep beam-spoiler impact the energy deposition is basically done by ionization.

We have recalculated the instantaneous temperature rise in the energy spoiler by the deep impact of a full train using the Montecarlo code FLUKA [45], considering the spoiler geometry of Fig. 34. The input is a train with 312 bunches, 3.72×10^9 particles per bunch, 1.5 TeV beam energy, and transverse beam sizes at spoiler $\sigma_x = 796\ \mu$m and $\sigma_y = 21.9\ \mu$m. No energy spread has been assumed. Fig. 35 shows the instantaneous temperature rise through the longitudinal section of the spoiler. We have obtained a maximum increment of temperature of about 280 K, which is below of the melting limit (1267 K) and even below of the thermal fracture limit (370 K). Therefore a Be based spoiler could withstand the impact of the full bunch train.

Unlike the energy spoiler, the betatron spoilers have been designed to be sacrificial, i.e. they would be destroyed if they suffer the direct impact of a bunch train. A possible alternative

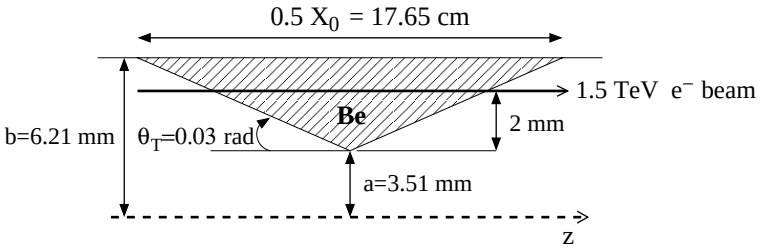

Figure 34: Schematic of the Be based energy spoiler for CLIC. The figure is not to scale and the taper angle has been exaggerated.

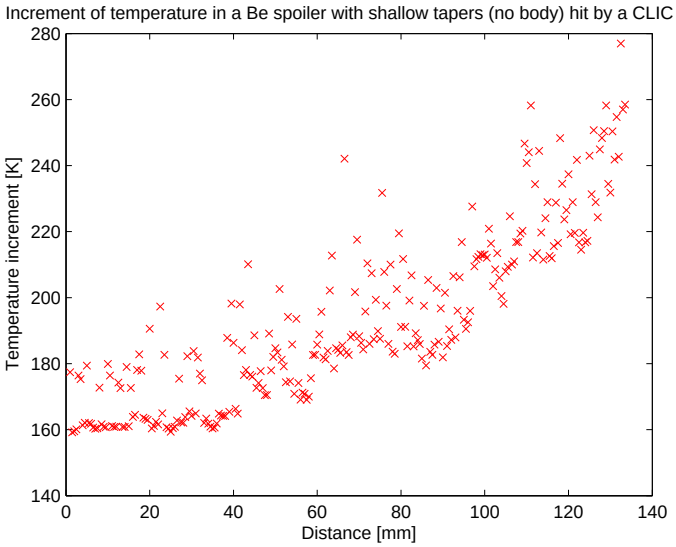

Figure 35: Instantaneous increment of temperature in a Be spoiler by the impact of an entire bunch train in CLIC.

is the use of rotating consumable collimators [46] as betatron spoilers for CLIC.

9.3 Collimation Efficiency

As we have already mentioned above, the CLIC collimation system consists of two parts: an energy collimation system and another section, downstream of the former, dedicated to beam halo cleaning in the transverse phase space. Here we present some preliminary results of collimation efficiency of the two systems.

9.3.1 Energy collimation

The energy collimation system fulfils a machine protection function against incoming errant beams. The goal is to spoil mis-steered beams coming from the linac with large momentum error $\gtrsim 1.3\ \%$.

We have study the efficiency of this system by means of beam tracking simulations using the code PLACET [47]. Gaussian distributions of 10^5 off-energy macroparticles are tracked through the BDS lattice. In this simulations the spoiler is treated as a “black” collimator, i.e. any macroparticle interacting with the aperture is assumed to be completely absorbed without secondary particle production. Fig. 36 shows the relative number of lost particles versus the average beam energy offset. We have compared three cases with different width energy spread

(assuming a Gaussian energy spectrum): $\sigma_E = 0\ \%$ (monocromatic beam), $\sigma_E = 0.25\ \%$ and $\sigma_E = 0.5\ \%$. The system seems to work as expected. For average energy offsets $\gtrsim 1.3\ \%$ practicaly the $100\ \%$ of the particles of the beam are removed by the energy spoiler. It is worth mentioning that with $0\ \%$ average beam energy offset and $\sigma_E = 0.5\ \%$ the results have shown $\sim 1\ \%$ of losses. This situation of losses during normal operation (nominal energy beam and $\sigma_E \approx 0.5\ \%$) has to be minimised in order to reduce the muon background at the IP. For instance, if we take into account that muons may be generated at a rate of about 10^{-4} per lost electron/positron and a $1\ \%$ of the beam particles hits the spoiler, then 0.01×312 bunches $\times$ 3.72×10^9 particles/bunch $\times\ 10^{-4} \simeq 1.16 \times 10^6$ muons/bunch train might be produced, which would actually be a quantity non-acceptable in terms of background at the IP.

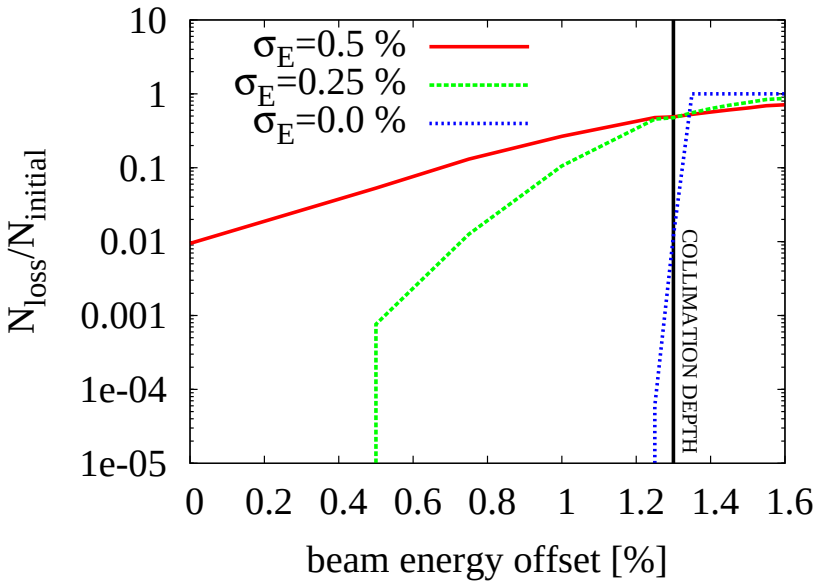

Figure 36: Relative beam particle loss at the energy spoiler versus the average energy offset of the beam. The curves correspond to the cases with beam energy spread $0\ \%$, $0.25\ \%$ and $0.5\ \%$. The vertical solid black line indicates the limit of the energy collimation depth.

9.3.2 Betatron collimation

The function of the betatron collimators is to clean the transverse beam halo, i.e. to clean particles with amplitudes $\gtrsim |\pm 10\ \sigma_x|$ and $\gtrsim |\pm 44\ \sigma_y|$ in the phase spaces x-x' and y-y', respectively.

To determine the cleaning efficiency of this system particles travelling at high transverse amplitude has been tracked using the code PLACET. We have used a simple halo model, which consists of macroparticles distributed in rings or ellipses of different radius: 10000 macroparticles per ellipse, and a Gaussian energy distribution with a mean energy value of 1.5 TeV (nominal energy) and a width energy spread of $0.5\ \%$. Here we have also assumed "black" spoilers.

Fig. 37 shows the particle loss as a function of the radius of the halo ring. For a horizontal halo (Fig. 37, left), with $\sigma_{y,y'}$ fixed at the nominal value, about a $20\ \%$ of the halo is removed at radius $10\ \sigma_{x,x'}$ (horizontal collimation depth) and the $100\ \%$ is removed for radii $\gtrsim 15\ \sigma_{x,x'}$. For a vertical halo (Fig. 37, right), with $\sigma_{x,x'}$ fixed at the nomimal value, about a $20\ \%$ of the halo is removed at radius $44\ \sigma_{y,y'}$ (vertical collimation depth), and the $100\ \%$ is removed

for radii $\gtrsim 70\ \sigma_{y,y'}$. All these losses are well localized at the betatronic spoilers. However, it is important to point out that no multiple Coulomb scattering has been considered. One would expect an increase of number of losses at nominal collimation depth radii $10\ \sigma_{x,x'}$ and $44\ \sigma_{y,y'}$ by mean of multiple Coulomb scattering in the spoiler and subsequent absortion in the downstream absorbers.

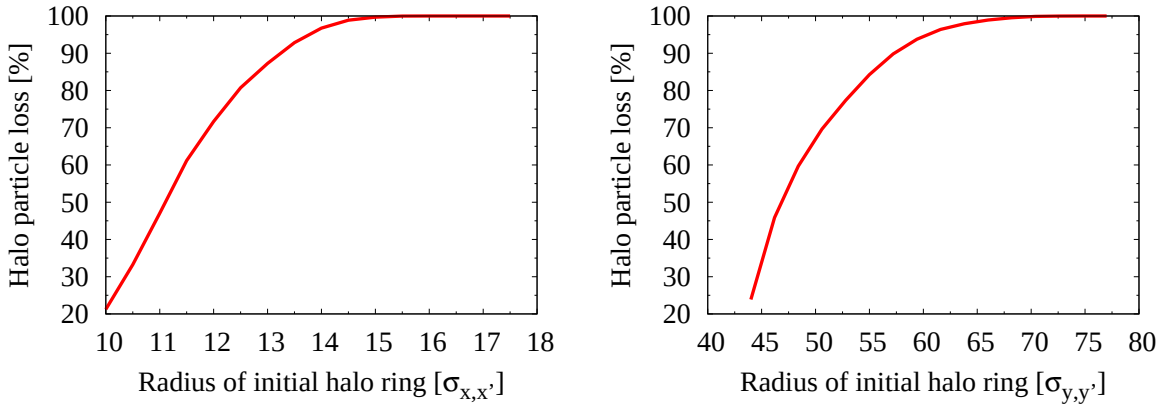

Figure 37:

More realistic halo models would be useful as an input for the cleaning efficiency studies. The different mechanisms for halo and tail generation should be better understood. Simulation results on halo and tail generation in the CLIC BDS have been presented in [48, 49]. In addition more realistic simulations should also include the energy deposition in spoilers and absorbers with secondary particle production and the collimator wakefield effects on the halo. Recently an interface of the codes PLACET and BDSIM has been developed which allows tracking studies including all these ingredients (see for example [50]). Further studies for the optimisation of the CLIC collimation efficiency need to be done.

9.4 Collimator Wakefield Effects

CLIC collimator wakefields have previously been studied using the tracking code PLACET [51] with collimation depths $10\ \sigma_x$ and $83\ \sigma_y$. Since the new vertical collimation depth has been reduced to $44\ \sigma_y$, we have recalculated the effects of the collimator wakefields on the luminosity.

The luminosity loss due to the horizontal misalignment of each horizontal spoiler and absorber is shown in Fig. 38. In comparison with the betatron collimators the energy spoiler (ENGYSP) and the energy absorber (ENGYAB) have been set with a big half-gap (see Table 12), and practically do not contribute to the luminosity degradation by wakefields. On the other hand, for the horizontal betatron spoilers we have obtained a misalignment tolerance of about $5/2\sigma_y \approx 20\ \mu$m ($10\ \%$ luminosity loss), which can be achieved with conventional survey alignment techniques.

More critical for the luminosity performance is the beam stability in the y-y' phase space, which is more sensitive to errors due to the transverse flatness of the beam ($\sigma_y^*/\sigma_x^* \simeq 1/50$). Fig. 39 shows the relative luminosity as a function of the bunch-collimator offset for each vertical betatron spoiler. The wakefields impose collimator misalignment tolerances of about $1/2\sigma_y \approx 1\ \mu$m ($10\ \%$ luminosity loss).

Fig. 40 compares the relative luminosity versus an initial vertical position jitter at the entrance of the BDS with collimator wakefields and without collimator wakefields. In this case the join effect of all the BDS collimators has been considered. The collimator wakefields impose

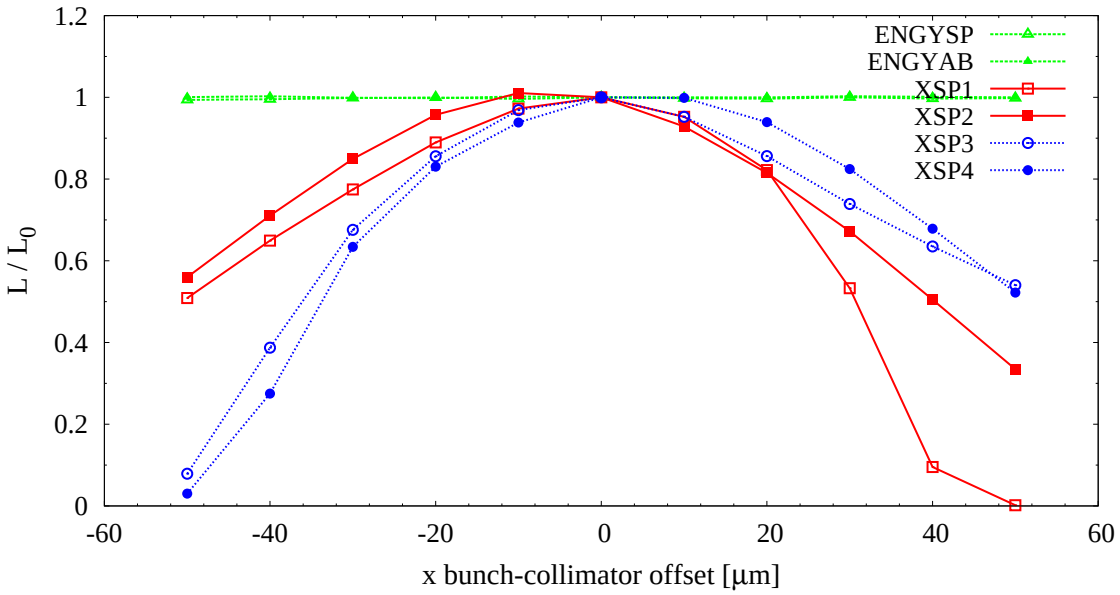

Figure 38: Luminosity loss versus horizontal bunch-collimator offset.

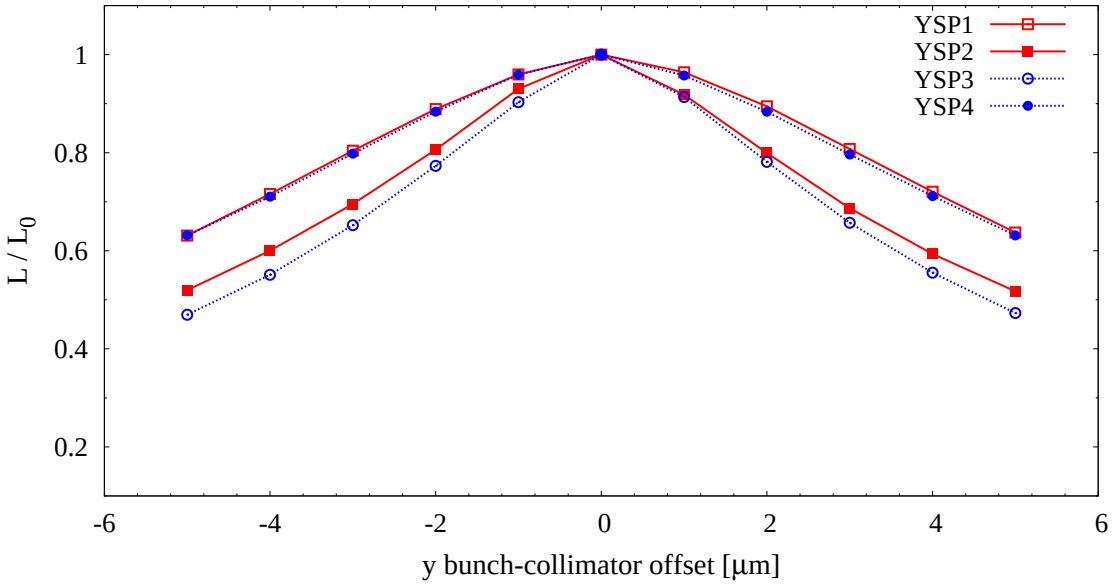

Figure 39: Luminosity loss versus vertical bunch-collimator offset.

an very tight initial jitter tolerance of about $0.2\ \sigma_y \approx 0.1\ \mu$m ($10\ \%$ luminosity loss). According to this simulation, if the jitter of the beam is $1\ \sigma_y$ at the entrance of the BDS, assuming no collimator wakefield, a $85\ \%$ of the nominal luminosity might be achievable; while with collimator wakefields effects, only a $65\ \%$ of the nominal luminosity.

We can conclude that in order to achieve the target luminosity, a collimator alignment in the vertical position with precision better than $1\ \mu$m will be required. Moreover, the jitter position of the incoming beam at the entrance of the BDS should be corrected at the submicrom level, for example by mean of precise orbit steering feedback systems using cavity beam position monitors and stripline kickers.

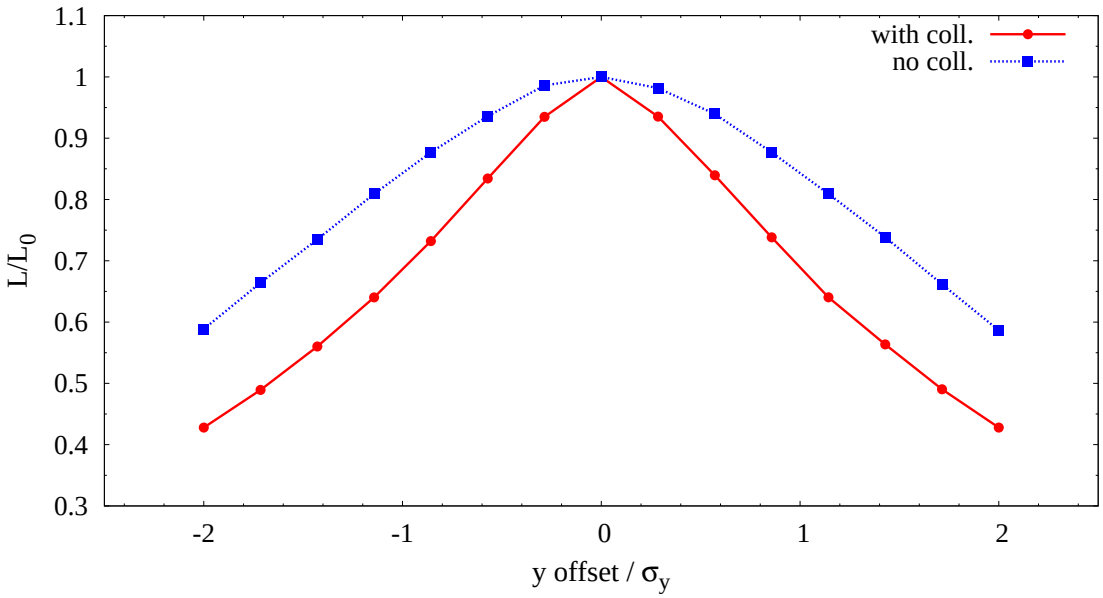

Figure 40: Luminosity loss versus initial jitter offset at the entrance of the BDS.

10 Damage simulations for CLIC and ILC spoilers and ATF2 tests

Presenter: Juan Luis Fernandez Hernando

The mission of the spoiler for the CLIC energy collimators in the BDS is to protect the main absorber by dispersing the beam, via multiple Coulomb scattering, in case of a direct hit. This will reduce the beam energy density and therefore avoid severe radiation damage. To ensure that dispersion the beam must traverse at least 0.5 radiation lengths of material at any point.

The spoiler effect on the beam during normal operation due to wakefield effects has to be reduced to a minimum. To achieve that, both the geometric contribution as well as the resistive contribution to the wakefield need to be minimised. A geometry with shallow leading and trailing tapers is used to reduce the impact on the geometry contribution and a high conductive material is recommended for the latter one. Therefore the first geometry considered has tapers with an angle of 0.03 radians and a center flat section of 0.5 radiation lengths of material. The material best suited for the tapers must be highly conductive as well as practically transparent for the beam, therefore present a large radiation length, to minimise the deposition of energy and avoid potential damage from the beam. Beryllium was selected for this purpose. For the flat section the requirement is to have a material with high conductivity as well as high fracture and melting temperature points. The options considered in this study are Titanium alloy (Ti6Al4V) and Beryllium. The alloy is more resistive than the Beryllium but its shorter radiation length, allowing for a shorter spoiler geometry, combined with its high fracture and melting points make it a good option. Beryllium tapers with Titanium alloy core is the most probable option for the ILC betatron collimation system spoiler design in the BDS as it could survive direct bunch hits at the same time that it allows for a reduction of length. As length does not seem to be an issue in the CLIC BDS the option with the Beryllium flat top presents the additional advantage of a better wakefield performance. Figure 41 shows the geometry used with a flat top made of Titanium alloy. The Beryllium option flat top would have a length of 17.65 cm instead of the 1.8 of the alloy.

The spoiler design has to survive the impact of the 312 bunches from the train. Each

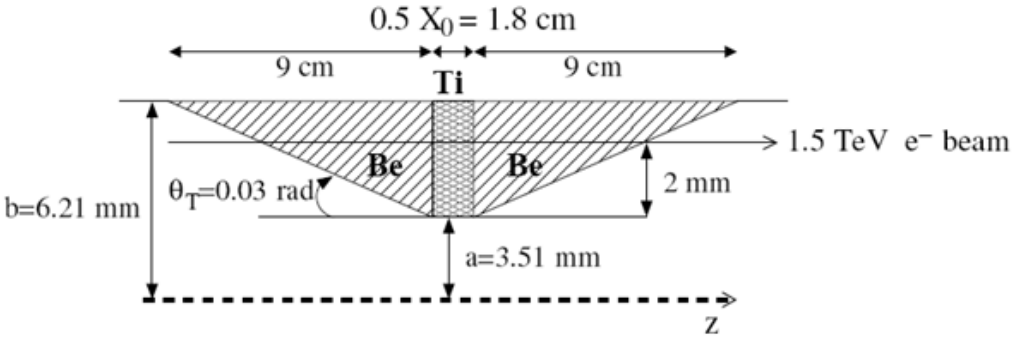

Figure 41: Spoiler with flat top made of Titanium alloy.

bunch is composed of 3.72E9 electrons at an energy of 1.5 TeV. The horizontal and vertical beam sizes at the spoiler's position is 796 and 21.9 microns respectively. That kind of impact was simulated for both options using FLUKA [52, 53]. Figures 42 and 43 show the temperature increment along its course inside the spoiler material due to a train of bunches hitting at the same position (i.e. without jitter), 2 mm from its top as shown in Fig. 41. This temperature increment it is the maximum one and is located in a volume of material surrounding the beam. The Beryllium spoiler, Fig. 42, will not reach melting temperature (1267 K) but it will reach fracture temperature (370 K) in the trailing taper. The Titanium alloy flat top of the other spoiler option, Fig. 43, would probably surpass fracture temperature (1710 K) and it is close to its melting temperature of 1941 K. In this case the trailing taper, made out of Beryllium, will reach its fracture point as well.

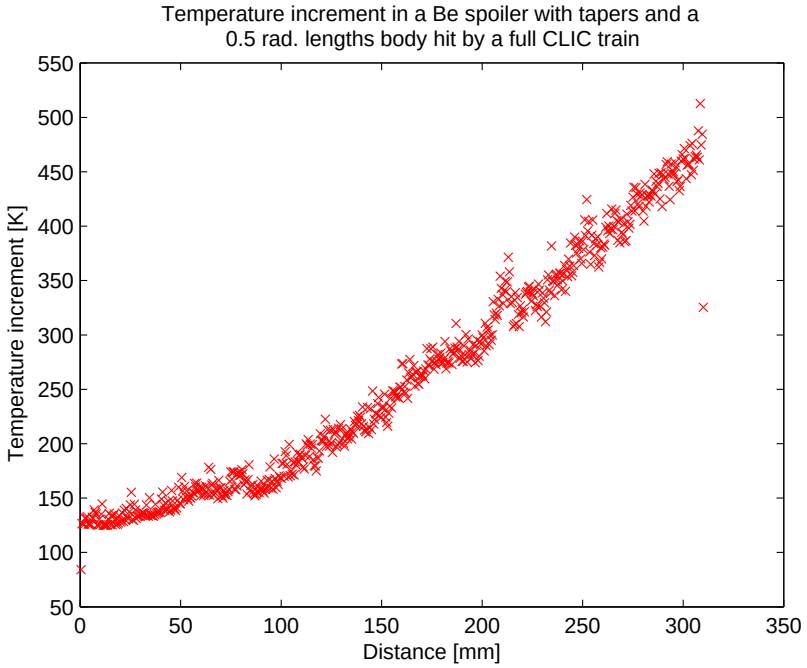

Figure 42: Temperature increment inside the Be spoiler material.

While it is relatively clear what reaching melting temperature on the spoiler would suppose: material being blown into the vacuum vessel, irregularities on the surface of the spoiler,

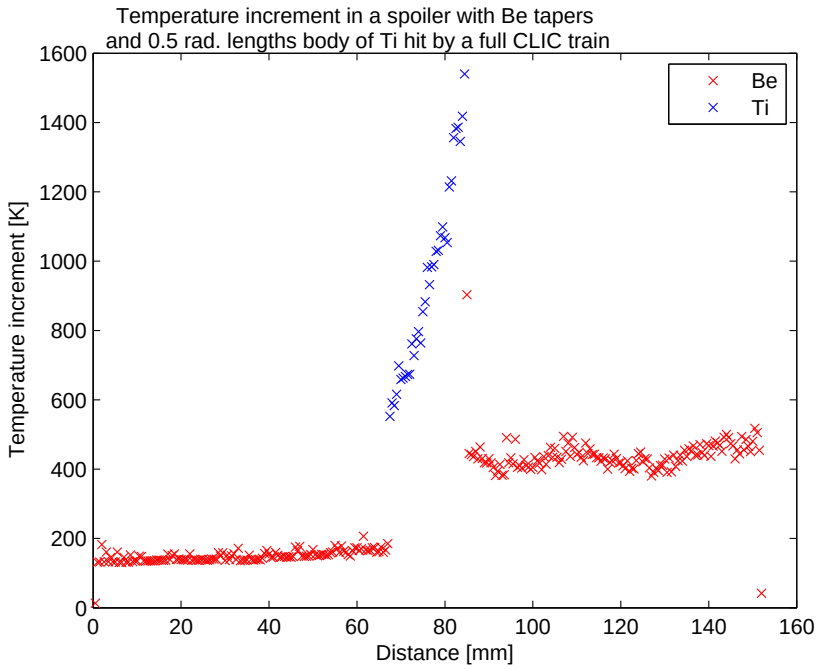

Figure 43: Temperature increment inside the Titanium alloy spoiler.

etc; it is not clear what the effects of a micro-fracture would imply. Therefore further studies are needed to understand the effect of fractures on spoiler properties as well as research other spoiler configurations that would allow full survivability. This studies should be done in parallel with a wakefield study to optimise the design, both using numerical codes and test beam experiments, as have already been done for the ILC spoilers [54]. Also studies of activation and residual equivalent dose rate once prototypes start to be designed. Another issue would be the design of a system that would detect damage in the spoilers.

11 CLIC collimation depth studies

Presenter: Frank Jackson, Daresbury

Collimation depths for CLIC are currently estimated at $10\sigma_x$ and $44\sigma_y$. This estimation has evolved from calculations done some years ago[2]. Here, these calculations are repeated for the up-to-date IP parameters and final doublet design in 2008. The nominal 3 TeV centre of mass energy is assumed.

The criteria constraining the collimation depth is that synchrotron radiation from the halo must pass cleanly through the interaction region. In the CLIC final focus designs, the small aperture permanent magnets (as small as 4mm in radius) impose the tightest constraints in the interaction region.

The collimation depth for the current CLIC compact final doublet (L* = 3.50m) is seen in Fig. 44 and is $23.2\sigma_x$, $69.9\sigma_y$. It can be seen that the aperture of QD0 determines the collimation depth.

Due to the significant dispersion in the CLIC final doublet, the horizontal collimation depth must be reduced by a factor of $\sqrt{2}$, giving $16.4\sigma_x$. The collimation depth calculated here is an upper bound, and may need to be reduced to provide a safety margin. Machine protection issues, not studied in detail yet, may also impact the collimation depth.

The collimation depth for the L* = 4.30m final doublet design may be somewhat looser,

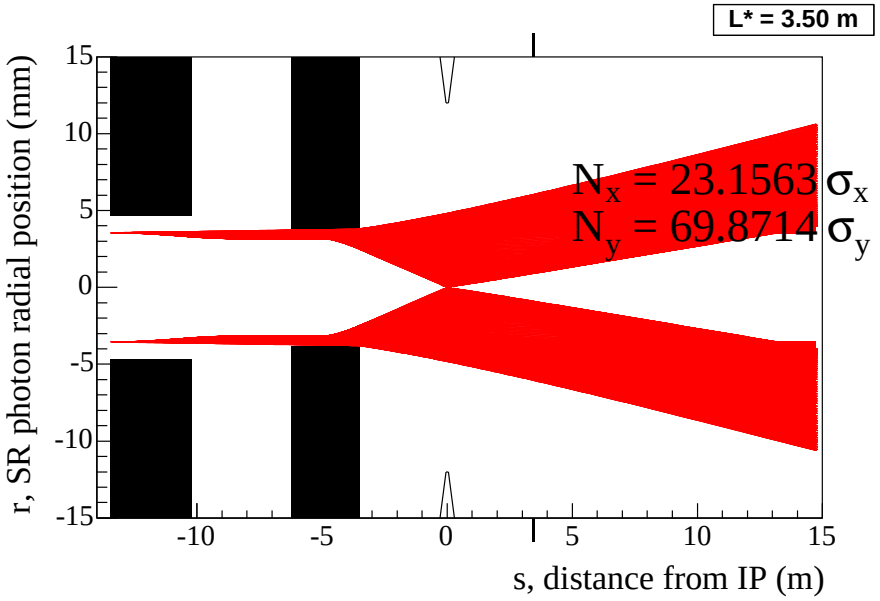

Figure 44: Collimation depth for the current CLIC compact final doublet (L*=3.5m).

since the QD0 aperture is 6.77 mm.

12 On a possibility of much shorter collimation system for CLIC

Presenter: Andrei Seryi, SLAC

Design of CLIC BDS and its collimation is based on damage threshold analysis [43] which includes Ohmic heating and standard dE/dz energy loss. However, recent observations at SLAC have shown that for CLIC short bunches there may be new effects that need to be taken into account.

Recent experiments devoted to studies of excitation of solid materials by ultra-short bunches [55], conducted at SLAC on FFTB, have shown a new effect that may be relevant for design of the CLIC collimation system. In this experiment, magnetized samples were placed under the 30GeV beam with 100fs to 5ps duration, and demagnetization due to field of the short bunch was studied. Typically, a localized damage was observed in the center of demagnetization pattern, due to the beam. The size of the damage was ten to thirty microns, which is close to the transverse size of the beam. In this study the new effect was observed: while there was damage of a sample observed for 4ps beam, this damage disappeared for a shorter 140fs beam.

A possible explanation of damage disappearance suggested by authors in [55] is that for short bunches the field gradient exceeds 2.5V over 0.25nm (which is typical distance between atoms) so that potential wells around each atom shift, and conduction zones do not overlap any more. Therefore, potential gradient leads to breakup of conduction path, there will be no current and correspondingly no heat transfer and no damage. (The energy still goes into the material, but is probably dissipated via emission of terahertz photons).

This phenomenon, if it is confirmed for CLIC-like beam parameters, may allow smaller beams at spoilers and thus shorter CLIC collimation system. Presently it is not clear how far the threshold is moved out, and the multi-bunch effects are to be understood also. A new experimental test, at facility like proposed FACET, would be helpful to explore this phenomenon further and to understand its applicability for design of a shorter collimation system for CLIC.

13 Spin Rotation Issues in CLIC

Presenter: Ken Moffeit, SLAC

13.1 Introduction

A description of CLIC and a parameter set is given in reference [10].CLIC produces longitudinal polarized electrons at the source. It is important to preserve the degree of polarization as the electrons travel from the source to the e^+e^- interaction region and to measure the polarization near the IR. The degree of polarization at the IR should be $0.99P_{e^-}^{xource}$.

13.2 Spin Rotation upstream of the Damping Ring

Longitudinally polarized electrons are produced from a GaAs cathode using circularly polarized photons. The helicity of the electron spin is selected for each pulse train by choosing the Pockels cell voltage producing left- or right-handed laser light. Only spin components perpendicular to the plane of the damping rings at E=2.424 GeV will be preserved. A spin rotation system is needed before the damping ring to orient the longitudinal electron spin to the vertical. The spin direction can be rotated normal to the damping ring using a Wein filter near the source where the electron beam energy is lower than 5 MeV. Crossed electric and magnetic fields in the Wein filter rotate the spin to the vertical while leaving the momentum direction unchanged. This was done at Jefferson National Lab for their polarized electron beam physics experimental program [56] and has also been proposed for ILC [57]. 3. Spin Rotation after the Damping Ring The spin vector must be oriented before the beam enters the main linac so that at the e+e- interaction region the spin is pointed in the desired direction, e.g. longitudinally polarized. The present plan at CLIC is to make the spin rotation after the damping ring where the beam energy is 2.424 GeV. A cartoon of the CLIC systems is shown in figure 1. After the damping ring there are:

- 90° bend where the beam energy is 2.424 GeV,
- 90° bend after the booster linac (beam energy 9 GeV) ,
- 180° bend after the beam is transported 24 km to the beginning of the main linac.

The spin precesses ahead of the change in momentum direction by an amount given by

$$\theta_{spin} = \gamma\frac{g-2}{2}\theta_{bend} = \frac{E(GeV)}{0.44065}\theta_{bend} \tag{20}$$

An energy spread of the beam in the 90 degree and 180 degree bends will result in spin diffusion and a depolarization of the beam. The goal is to have PIR 0.99 Œ PeSource , which - gives limits for the acceptable energy spread in the transport system. Keeping spin diffusion effects small is also important to limit systematic errors in determining the luminosity-weighted polarization due to chromatic effects.

Option A: Spin rotation at 2.424 GeV is located directly after the damping ring and before bunch compression, BL1. The energy spread in the damping ring is 0.134%, but, the energy spread after the bunch compressor may be much larger. In order to keep depolarization small due to spin diffusion the energy spread of the 2.424 GeV beam after the bunch compressor must be less than 1.9% as the beam is deflected 90 degrees into the Booster Linac.

Option B: Spin rotation at 2.424 GeV is located after the 90 degree bend and before the Booster Linac. The spin direction is normal to the 90 degree bend and therefore is not depolarized. The beam then enters the spin rotation system. The first solenoid system rotates the spin from the vertical to transverse horizontal. Depolarization due to spin diffusion will

be small for energy spreads less than 6%. After the first solenoid a $\approx 16.36^{\circ}$ bend rotates a horizontal transverse component to a longitudinal component and requires an energy spread less than 6% to keep the depolarization losses small. Option A and B: There are also constraints on the energy spread after the booster linac where the beam energy is 9 GeV for both options A and B. At the end of the 24 kilometer transport system there is 180 degree bend, which can be considered as two 90 degree bends. The first 90 degree bend orients the beam back to the direction of the booster linac. As a result any spin diffusion effects due to the 90 degree bend at the end of the booster linac is canceled by this 90 degree bend. So we need only consider spin diffusion depolarization effects due to a 90 degrees bend at 9 GeV. Presently, the CLIC parameters show an energy spread of 1.3% at 9 GeV [10]. Figure 45 shows the spin diffusion and depolarization from a 90 degrees bend at 9 GeV with a 1.3% energy spread.

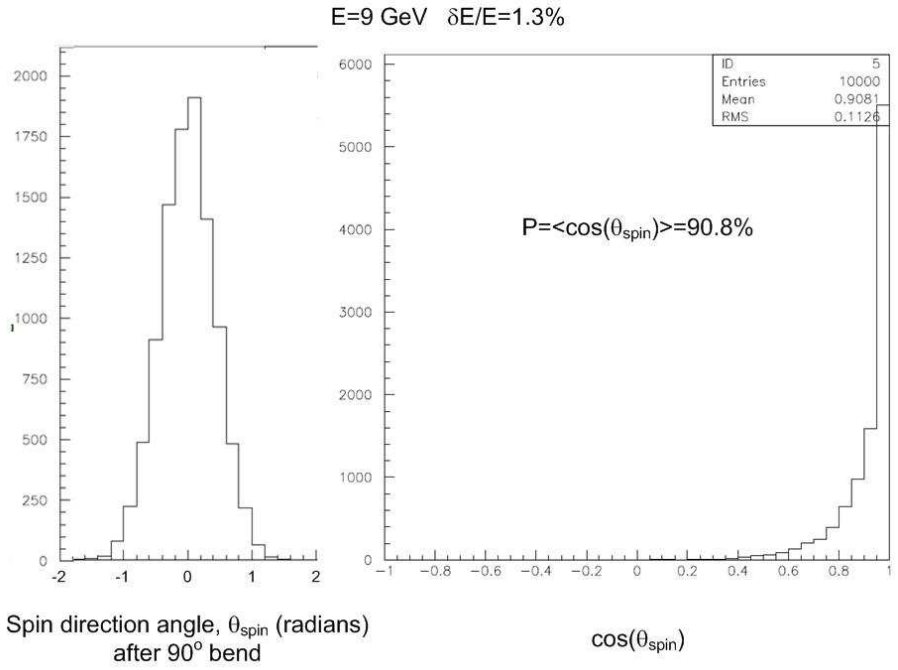

Figure 45: Spin direction and average polarization after 90° bend at 9 GeV with 1.3% energy spread.

The spin direction extends out to ± 1 radian about the nominal direction and gives a mean depolarization of 9.2%. Table 13 gives the mean longitudinal or transverse horizontal polarization after a 90 degrees bend for different energy spreads.

The energy spread at 9 GeV will need to be less than 0.5losses of the longitudinal and transverse horizontal polarization spin components in a 90 degrees bend.

Option C: If the energy spreads at 2.424 GeV and 9 GeV are too large the spin rotation can be done at 9 GeV after the reverse bend and before the beam is injected into the main linac. The polarization is in the vertical direction during the 90 degrees bend, 24 km transport line and 180o bend and depolarization effects will not occur. The insert in figure 1 shows the spin rotation elements required at 9 GeV:

- a flat-beam spin rotation system proposed by Paul Emma [58], which, includes half solenoids with a reflector beam line between them to eliminate cross plane coupling,
- focusing elements to remove the focusing effects of the solenoids,
- Four superconducting solenoids of strength 23.1 Tm.

δE/E at 9 GeV	$< P >$ Mean longitudinal or transverse horizontal polarization after 90 deg bend (note: a vertical spin component will not be depolarized)
0.25%	99.6%
0.5%	98.6%
1.0%	94.0%
1.3%	90.8%

Table 13: Spin diffusion effects for different energy spreads at 9 GeV.

– A 4.4065° bend is required between the first and second spin rotation systems. This allows for all three components of the spin to be injected into the main linac so that the desired polarization is achieved at the IR.

Spin diffusion is small in the spin rotation system at 9 GeV with a 1.3% energy spread and will not depolarize the beam. The bottom line is that the transport system between the polarized electron source and the e+e- interaction region should be designed to transmit greater than 99% of $P_{e^-}^{Source}$.

13.3 Compton Polarimeter

A Compton polarimeter has been proposed upstream of the interaction region in the beam delivery system [59]. The angle of the beam at the Compton IP and at the interaction region should be the same in the horizontal and vertical directions. The tolerance on the difference should be less than 20μrad due to the large $\gamma(g-2)/2$ at 1.5 TeV.

$$\theta_{spin} = \gamma\frac{g-2}{2}\theta_{bend} = \frac{E(GeV)}{0.44065}\theta_{bend} = 3404.06\theta_{bend}\ at\ 1.5TeV \tag{21}$$

It will also be necessary to monitor the beam direction at both places with beam position monitors.

13.4 Extraction Line Polarimeter

Presently, the CLIC design does not have extraction line polarization and energy measurements. The 20 mrad crossing angle at CLIC in principle allows for an ILC type extraction line polarimeter and energy measurement. Figure 46 shows the elements of the ILC extraction line energy spectrometer and polarimeter [60]. There are significant difficulties for an extraction line polarimeter at CLIC.

For beam energies below 500 GeV, the beamstrahlung photons and disrupted electron beams in the extraction line will be similar to those in the ILC design. Extraction line energy and polarization measurements would therefore be possible and would provide important independent measurements and calibration for the upstream polarimeter and energy measurement instruments. They could also help understand the luminosity weighted polarization. At higher beam energies, the polarization could also be measured from beams out of collision at a low rate

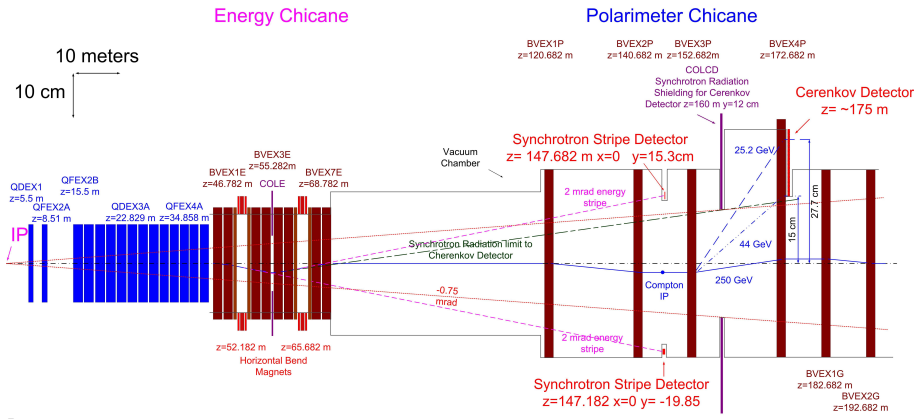

Figure 46: Schematic of the ILC extraction line energy measurement system and the Compton polarimeter.

of ≈1 hertz if backgrounds are large. There are significant concerns about placing instruments in the extraction line at CLIC, however:

- At the highest CLIC energies the very large beamstrahlung momentum spread and beamstrahlung photons per electrons will require a larger beam stay-clear than the 0.75 mrad at the ILC requiring larger aperture magnets.
- The large beamstrahlung momentum spread of 29% may not allow a focusing system for a small beam size at the Compton IP and have acceptable beam losses in the extraction line.
- The higher energy beams of 3 times that of ILC will require longer magnets to obtain the desired deflections in the energy and polarimeter chicanes.
- Without focusing elements the beam size will be large at the Compton IP even with beams out of collision requiring high power laser for an adequate Compton backscatter rate. The CLIC divergence is 6 rad in the horizontal and 14 rad in the vertical giving a beam size of 1.2mm by 2.8mm at 200m from the IR. This gives a larger area by a factor of 340 than that at the ILC. The number of particles per bunch is smaller by a factor 2 at CLIC (0.37×10^{10}) over ILC (0.75×10^{10}). The laser power would need to be a factor 700 times larger in a CLIC Compton polarimeter to obtain the same number of Compton electron of 300/cm detected as in the ILC polarimeter [60].
- Without focusing the transfer matrix between the IR and the Compton IP will not be optimal (R22=-0.5) for extracting the luminosity weighted polarization.

The improvements with instrumentation in the extraction line to allow precision measurements of polarization and energy at CLIC warrant more study.

13.5 Laser Wire Detector

A study for the ILC showed that synchrotron radiation backgrounds in 0-degree line will give unacceptably large backgrounds in a photon laser wire detector [61]. A preferred solution is to detect the Compton-scattered electrons.

13.6 Positron Polarization

Presently the CLIC design does not include a polarized positron source. Similar design criteria as given for polarized electrons will apply to positron polarization if that option

is included in the future. The spin rotation and helicity selection before the damping rings for polarized positrons would occur 400MeV after positron capture and pre-acceleration [57].

14 Alignment studies: Decelerator and CTF3

Presenter: Erik Adli, CERN

The Compact LInear Collider (CLIC) study has shown that advanced beam-based correction will be needed in order to ensure nominal performance for several parts of the collider, including the Decelerator [62]. The CLIC Test Facility 3 (CTF3) has been constructed at CERN in order to demonstrate feasibility of several key concepts of CLIC. The CTF3 linac is fully loaded [63], implying that current jitter leads will lead to significant energy jitter - analogous to the Decelerator and the TBL, and the linac was therefore selected as test-case for beam based correction [64]. In particular Dispersion-Free Steering (DFS) [65] was tested, and compared to All-to-All correction.

For the nominal linac, consisting of 11 triplet cells, All-to-All correction gave as good results as DFS (residual dispersion ≈5mm). In order to verify the performance of Dispersion DFS, a test-case with simulated large BPM offsets was defined. The position bump leads to a factor three higher dispersion after the bump (15 mm).

Figures 47 and 48 show the position measurement and dispersion measurement, respectively, after All-to-All correction and Dispersion Free Steering have been peformed on the real CTF3 linac, with the simulated BPM offsets active.

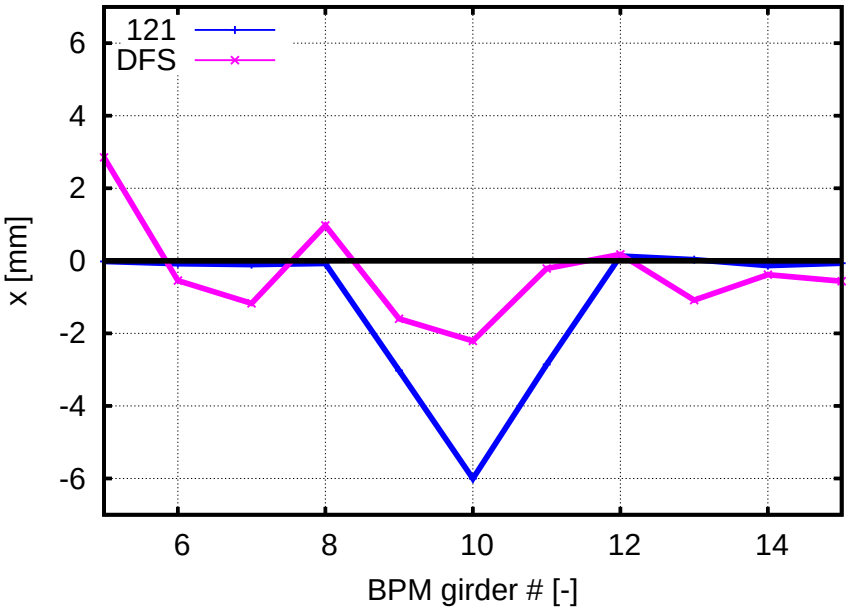

Figure 47: Position measurement after all-to-all correction and dispersion free steering in CTF3.

We observe that DFS has indeed managed to reduce the disperison by a factor ≈3 (to ≈5 mm, the minimum achieved without the bump as well). In addition we note that DFS is mostly oblivious to the BPM readings (the difference of the nominal and the dispersive orbit is given large weight). This means that in practice DFS can also give indications where problems are located.

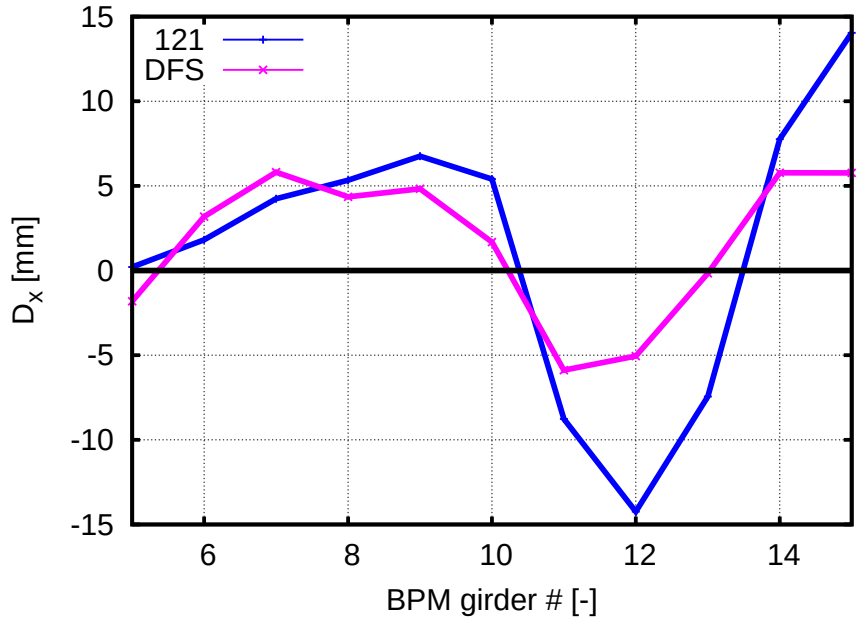

Figure 48: Dispersion measurement after all-to-all correction and dispersion free steering in CTF3.

15 ATF2 Final Doublet Support

Presenter: A. Jeremie, LAPP[1)]

15.1 Introduction

The ATF2 Final Doublet (FD) is situated at the end of the ATF2 final focus section comprised of two quadrupoles (named QD0 and QF1), two sextupoles (SD0 and SF1) and corresponding cavity BPMs (Beam Position Monitors). The Final Doublet is set just in front of dedicated instrumentation including a Shintake Monitor giving the size of the electron beam. The distance separating the farthest SF1 magnet center from the Interaction Point (IP) is 3,17m. The distance separating the most critical magnet QD0 from the IP is 1.23m. The present section describes the study for the FD support. The support needs to satisfy some requirements. Reference [66] shows that the QD0 magnet vertical jitter should not exceed 6-7nm to avoid a 2% increase in beam size. In addition, measurements of the ATF ground motion show that the ground vibrations diminish as the frequency rises. Above 100Hz, ground motion can be considered low enough. The low frequency limit is given by the ability for the Beam-Based feedback to compensate for beam instabilities. Since the beam repetition rate is 1Hz, the beam based feedback will work only below a fraction of this frequency, i.e. around 0.1Hz. The desired frequency range is thus 0.1Hz-100Hz. The support should be able to evolve as Final Focus design evolves. In addition, it needs to adjust the magnet position to a beam height of 1.2m. And finally, the relative jitter tolerance is 6-7nm. There are two possible approaches to the problem. One can either cut or reduce the vibrations in the frequency range of interest, or one can design the support in order to push the resonance peaks outside of the frequency range, in this case, to higher frequencies where the ground vibration is lower.

[1)] Work supported by the Agence Nationale de la Recherche of the French Ministry of Research (Programme Blanc, Project ATF2-IN2P3-KEK, contract ANR-06-BLAN-0027)

15.2 Initial design

Initially, the idea was to use a commercial active isolation system with a honeycomb block and active isolators that had proven to give excellent results within the CLIC tolerances [67], but was not satisfactory for the frequency range needed for ATF2 [68]. Another approach needed to be found. We want the measurement to have a coherent behaviour with respect to the beam. This means that the relative motion between the Shintake monitor (measuring the beam size) and the FD should have a maximum jitter of 6-7nm in the vertical axis above 0.1Hz. It also supposes that QD0 is rigid and does not have detrimental resonances. Vibration measurements on site at KEK have shown that ground motion is coherent up to 4m. This is slightly more than the distance separating the last FD magnet from the Shintake monitor. Thus, the chosen strategy was to study separate stiff supports for the FD and the Shintake Monitor in order to behave in the same way as ground motion. We continued studying the rigid honeycomb block but without the active isolators. In free-free configuration, this block has its first resonance frequency at 230Hz. A finite element (FE) calculation simulating a simple block (without the complex honeycomb structure) showed however that when the block is positioned on 4 supports at its corners, the first resonance peak drops to 56Hz, and even lower to 26 Hz, when the weight of the FD magnets is put on the block. These peaks are in the frequency range of interest. Vibration measurements confirmed these low frequency peaks, respectively 80Hz and 41Hz on the honeycomb block. To estimate the impact of these peaks on the relative motion between the FD and the Shintake Monitor on the KEK site, the Integrated RMS of relative motion between the block and the floor has been done. The calculation is performed by integrating the vibratory behaviour of the block measured at LAPP and the data of ATF ground motion [3]. Figure 49 shows the block transfer function for 3 different weights. The integrated rms from 0.17 to 100Hz is 6.7nm with the FD mass on the block. This is slightly above the 6-7nm tolerance needed. The impact of the peak alone at 41Hz is already of 5.7nm mainly because of it's low frequency position.

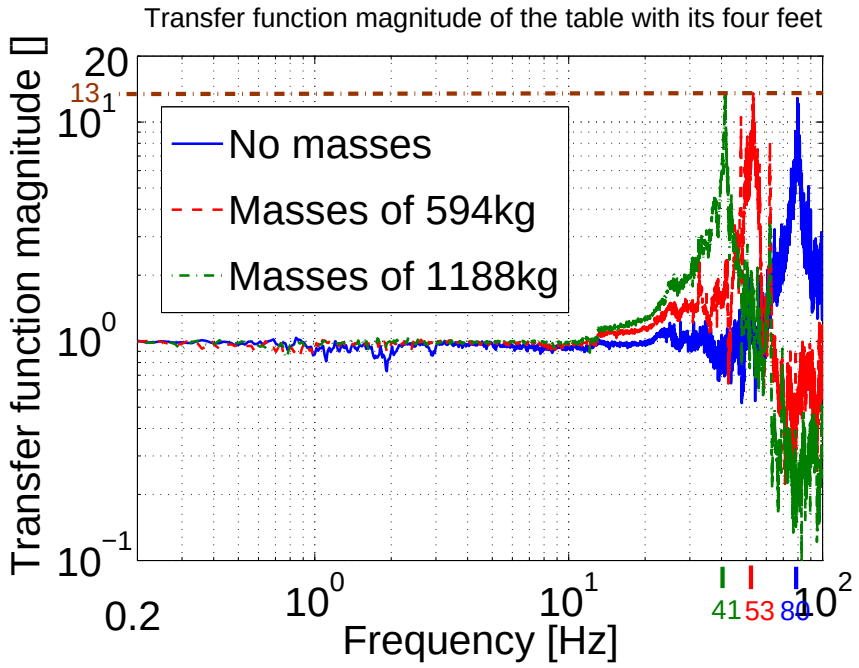

Figure 49: Transfer function of the honeycomb block for 3 different weights.

It has been shown in ref [3] that these peaks are not resonance peaks of the block, but

are due to the boundary conditions of the 4 feet. The rigid honeycomb block did not show any resonances in all 3 directions under 150Hz.

15.3 Current design

We need to push the peaks to higher frequencies. This can be achieved by fixing the block on its entire face to the floor instead of fixing it only at the corners. The FE calculation of the simple block gave encouraging results, namely 526Hz and 135Hz respectively without and with the FD weight. Since the FD support should allow for FD design evolution, the choice has been made to first fix steel plates to the floor with bolts and then fix the block to the plates with beeswax having good vibration transmission properties, can be easily unglued, is stable in time and is rad hard. Some additional design has been done to adjust in x, y, z with shims (0.05mm) and adjustment pushers for a 1.2m beam height. Vibration measurements confirm the good behaviour of the block completely attached to the floor. The peaks are respectively above 100Hz for the empty block (outside the measurement range), and 92Hz for the block with FD weight. Figure 50 shows the corresponding transfer function.

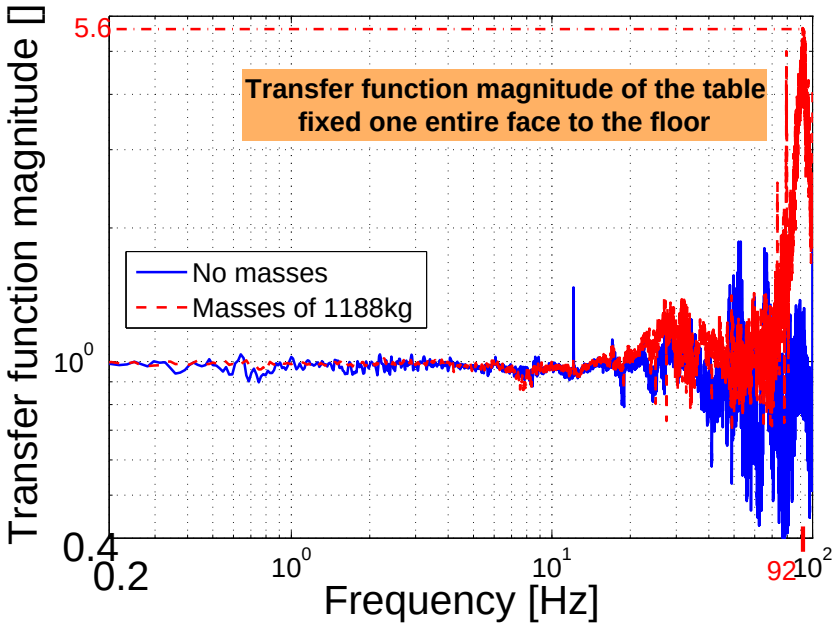

Figure 50: Transfer function of the current design of the FD support.

Table 14 shows the integrated rms for the peak for different measurements.

Object	Peak position	Integrated RMS
4-feet block with weight	41 Hz	5.7 nmm
Glued block with weight	92 Hz	0.3 nm
Sextupole on mover/support	100 Hz	0.15 nm
Quad on mover/support	76 Hz	1.1 nm

Table 14: Margin specifications

The sum of the integrated rms for the fixed block and magnets is below the 6-7nm jitter. The honeycomb block fixed to the floor on the whole surface, with adjusted movers has been validated for ATF2 FD support. Some additional vibration measurements with water flowing through the magnets have shown no significant impact on the vibrational behaviour of the support and magnets. The whole system has been shipped to KEK during August 2008, it has been installed, centered and aligned in x, y and z on Thursday September 25 2008 (see Fig. 51). The BPMs have been installed on October 15, 2008.

Figure 51: ATF2 final doublet.

The FD section is the fruit of a successful international collaboration since the different components come from several institutes: Quadrupoles, sextupoles and movers from SLAC (from FFTB), the support from floor to mover come from LAPP, the BPM+support from KNU and LAPP.

15.4 Conclusion

In conclusion, the ATF2 rigid Final Doublet support has been chosen (vs. active support), SLAC FFTB movers adjusted to meet beam height. Vibration measurements validate the rigid support choice, and Water flow in magnets has no significant effect on vibrations. Finally the ATF2 Final Doublet support is installed at KEK ready for the first beam to start before the end of the year 2008.

Acknowledgments

We are thankful to the CLIC08 Local Organising Committee for his excellent work and for having made CLIC08 possible.

K. Elsener would like to acknowledge the information and help received from A. Ferrari, V. Ziemann, R.B. Appleby, M. Salt, I. Ahmed, H. Braun, E. Bravin, L. Bruno, T. Lefevre, T. Otto, D. Schulte, R. Tomás, H. Vincke and T. Zickler.

Ken Moffeit thanks Mike Woods, Peter Schuler, Andrei Seryi and Takashi Maruyama for their contributions to his presentation at CLIC-08 and the preparation of this document.

References

[1] CLIC08 Workshop, CERN 14-17 October 2008:
http://project-clic08-workshop.web.cern.ch/project-clic08-workshop/

[2] R. Tomás, "Optimizing the CLIC Beam Delivery System", CERN-OPEN-2008-008; CLIC-Note-735 (2008).

[3] CLIC web lattice repository:
http://clicr.web.cern.ch/CLICr/MainBeam/BDS/

[4] M. Woods, K. Moffeit, "Synchrotron Backgrounds for Laserwire Detector in Upstream Polarimeter Chicane" ILC-Note-2008-041.

[5] P. Schuler, "Upstream polarimeter for CLIC" CLIC08
http://indico.cern.ch/getFile.py/access?contribId=291&sessionId=38&resId=0&materialId=slides&confId=30383

[6] M. Aleksa, S. Russenschuck, "STUDY OF SOME OPTIONS FOR THE CLIC FINAL FOCUSING QUADRUPOLE", CLIC Note 506 and CERN-OPEN-2002-009.

[7] S. Bai and P. Bambade, "Intermediate beta configurations at the IP for commissioning and optimisation" in the Fifth ATF2 project meeting:
http://atf.kek.jp/collab/md/projects/project_frame.php?project_page=1
and
M. Thorey, P. Bambade, "ATF2 variable β_{IP} parameters", LAL/RT 07-05:
http://publication.lal.in2p3.fr/2007/lalrt0705.pdf

[8] R. Tomás, "MAPCLASS: a code to optimize high order aberrations" CERN AB-Note-2006-017 (ABP), and "Non-linear Optimization of Beam Lines", Phys. Rev. ST Accel. Beams **9**, 081001 (2006).

[9] P. Tenenbaum "Expanded Studies of Linear Collider Final Focus System at the Final Focus Test Beam", SLAC-R-475:
http://www.slac.stanford.edu/pubs/slacreports/slac-r-475.html

[10] F. Tecker, *et al.*, "CLIC 2008 Parameters", CLIC-Note-764 (2008).

[11] ILC Reference Design Report:
http://lcdev.kek.jp/RDR/

[12] D. Schulte, "Beam-Beam Simulations of the Proposed ILC Parameters", EUROTeV-Memo-2005-004-1.

[13] P.Burrows et al, "Performance of the FONT3 fast analogue intra-train beam-based feedback system at ATF", EPAC 2006.

[14] G. Burt, R.M. Jones, A. Dexter, "Analysis of Damping Requirements for Dipole Wake-Fields in RF Crab Cavities." IEEE Trans. Nuc. Sci. Vol. 54, 2007.

[15] A. Dexter and G. Burt "Phase and Amplitude Control of Dipole Crabbing Modes in Multi-Cell Cavities", EUROTeV-Report-2008-064, 2008.

[16] G. Burt, A. Dexter , P. Goudket, A.C and A. Kalinin, "Effect and tolerances of phase and amplitude errors in the ILC Crab Cavity", EUROTeV Report 2006-098.

[17] J. W. Staples, R. Wilcox and J. M. Byrd, "Demonstration of femto-second phase stabilization in 2 km optical fibre", Proceedings of PAC07, Albuquerque, New Mexico, USA.

[18] D. Alesini, A. Gallo, B. Spataro, B. Marinelli A. and L. Palumbo L. Nuclear Instruments and methods in physics research A 580 (2007) 1176-1183.

[19] C. Nantista, S. Tantawi, and V. Dolgashev, "Low-field accelerator structure couplers and design techniques", Phys. Rev. ST Accel. Beams **7**, 072001 (2004).

[20] A. Ferrari, "Conceptual design of a post-collision transport line for CLIC at 3 TeV", EUROTeV-Report-2007-001, CLIC Note 704.

[21] A. Ferrari, "Impact of the new CLIC beam parameters on the design of the post-collision line and its exit window", EUROTeV-Report-2008-021, CLIC Note 739.

[22] M. Salt and R.B. Appleby, private communication.

[23] A. Ferrari, V. Ziemann, R.B .Appleby, M. Salt, "Conceptual design of a beam line for post-collision extraction and diagnostics at the multi-TeV Compact Linear Collider", submitted for publication in PRST.

[24] P. Eliasson et al, "Luminosity Tuning at the Interaction Point", EUROTeV-Report-2006-039, CLIC Note 669.

[25] V. Ziemann, "CLIC Post-Collision Diagnostics", EUROTeV-Report-2008-016, CLIC Note 736.

[26] E. Bravin, private communication (2007)

[27] D'Amico *et al., CERN/PS 2001-028 and PAC* (2001).

[28] http://www.slac.stanford.edu/accel/ilc/codes/dimad

[29] J. Payet et al., BETA code.

[30] K. Oide, *Phys. Rev. Lett.* **61** (1988) 1713.

[31] A. M. Chao, *Physics of Collective Beam Instabilities in High Energy Acceleratros*, John Wiley and Sons, New York, 1993

[32] K. L. F. Bane and M. Sands, *The Short Range resistive Wall Wakefields*, SLAC-PUB-95-7074 (1995)

[33] Wolfram Research Inc., Mathematica Version 6, Champaign, IL (2007)

[34] http://www.hep.manchester.ac.uk/u/adina/

[35] A. Bungau and R. J. Barlow, *Simulation of High Order Short Range Wakefields* WEPCH123: Proceedings of EPAC 2006, Edinburgh, Scotland (2006)

[36] A. Bungau and R. J. Barlow, *Wakefield Calculation - Comparison between Simulation and Experimental Data* MOPP007: Proceedings of EPAC08, Genoa, Italy (2008)

[37] G. Geschonke and A. Ghigo, "CTF3 Design Report", CERN/PS 2002-008 and LNF-02/008, 2002.

[38] I. Agapov et al, "Halo Estimates and Simulations for Linear Colliders", CERN-AB-2007-045 and CLIC-Note-714.

[39] H. Burkhardt et al, "Halo and tail generation studies for linear colliders" CERN-AB-2006-054 and CLIC-Note-668.

[40] D. Schulte and F. Zimmermann, "Failure Modes in CLIC", Proceedings of PAC2001, Chicago, USA, 2001; CLIC Note 492 (2001); CERN-SL-2001-034 (AP) (2001).

[41] F. Jackson, "CLIC Collimation Depth Studies", Talk given at the CLIC'08 Workshop, CERN, 14-17 October 2008.

[42] R. Tomás, private communication.

[43] S. Fartoukh, J. B. Jeanneret and J. Pancin, "Heat deposition by transient beam passage in spoilers", CERN-SL-2001-012 AP, CLIC Note 477, 2001.

[44] J. Resta-López and L. Fernández-Hernando, "Review of the CLIC Energy Collimation System and Spoiler Heating", EUROTeV-Report-2008-050 (2008).

[45] A. Fasso, *et al.*, "FLUKA: a multi-particle transport code", CERN-2005-10 (2005), INFN/TC-05/11, SLAC-R-773.

[46] J. Frisch, E. Doyle, K. Skarpaas, "Advanced Collimator Prototype Results for the NLC.", SLAC-PUB-8463 (2000).

[47] D. Schulte *et al.*, “Simulation Package based on PLACET”, PAC2001, Chicago, USA, 2001; CLIC Note 482 (2001); CERN/PS 2001-028 (AE) (2001), see the web site: https://savannah.cern.ch/projects/placet.

[48] H. Burkhardt *et al.*, “Halo Estimates and Simulations for Linear Colliders”, Proceedings of PAC2007, Albuquerque, New Mexico, USA, 2007; EUROTeV-Report-2007-064; CLIC-Note-714.

[49] Ijaz Ahmed, “Halo and Tail Generation”, Talk given at the CLIC’08 Workshop, CERN, 14-17 October 2008.

[50] S. Malton *et al.*, “Simulation of Beam Halo in CLIC Collimation Systems”, Proceedings of EPAC2008, Genoa, Italy, 2008; EUROTeV-Report-2008-01; see also S. Malton, “Collimator Studies”, Talk given at Final EUROTeV Scientific Workshop, Uppsala, Sweden 26-28 August 2008.

[51] G. Rumolo, A. Latina and D. Schulte, “Effects of the Wake Fields in the CLIC BDS”, Proceedings of EPAC2006, Edinburgh, UK, June 2006.

[52] A.Fasso, A.Ferrari, P.R.Sala, "Electron-photon transport in FLUKA: status", Proceedings of the MonteCarlo 2000 Conference, Lisbon, October 23–26 2000, A.Kling, F.Barao, M.Nakagawa, L.Tavora, P.Vaz - eds., Springer-Verlag Berlin, p.159-164 (2001).

[53] A.Fasso, A.Ferrari, J.Ranft, P.R.Sala, "FLUKA: Status and Prospective for Hadronic Applications", Proceedings of the MonteCarlo 2000 Conference, Lisbon, October 23-26 2000, A.Kling, F.Barao, M.Nakagawa, L.Tavora, P.Vaz - eds. , Springer-Verlag Berlin, p.955-960 (2001).

[54] J.L. Fernandez-Hernando, S. Molloy, J.D.A. Smith, N.K. Watson, "Measurements of collimator wakefields at End Station A". EUROTeV Report 2008-045 and EPAC’08 WEPP163 proceedings.

[55] J. Stohr (SLAC), et al, “Exploring Ultrafast Excitations in Solids with Pulsed e-Beams”, presented on Feb 19, 2008 at SLAC FACET review, http://www-group.slac.stanford.edu/ppa/Reviews/facet-review-2008/Agenda.asp

[56] J. Grames, “Measurement of a Weak Polarization Sensitivity to the Beam Orbit of the CEBAF Accelerator”, Joseph Michael Grames, Ph.D. Thesis, Department of Physics, University of Illinois at Urbana-Champaign, 2000.

[57] K. Moffeit, “Spin Rotation before the Damping Ring”, IPBI TN-2008-3, April 2008.

[58] Paul Emma, NLC-Note-7, December 1994.

[59] Peter Schuler, “Upstream Polarimeter for CLIC”, Talk presented at the CLIC-08 Workshop, October 2008

[60] K. Moffeit, “Downstream Extraction Line Polarimeter”, IPBI TN-2008-5, April 2008.

[61] M. Woods, et.al., ILC-Note-2008-041, March 2008.

[62] E. Adli and D. Schulte, “Beam-Based Alignment for the CLIC Decelerator”, *Proceeding of EPAC 2008* (2008)

[63] R. Corsini et al., First Full Beam Loading Operation with the CTF3 Linac, *Proceeding of EPAC 2004* (2004)

[64] E. Adli et al., “Status of an Automatic Beam Steering for the CLIC Test Facility”, *Proceeding of Linac 2008* (2008)

[65] T.O. Raubenheimer and R.D. Ruth, A dispersion-free trajectory correction technique for linear colliders, **NIM** A302 (1991) 191-208

[66] ATF2 Proposal, Vol. 1, ATF2 Group, August 11, 2005 (Revised January 23, 2006) CERN-AB-2005-035, KEK Report 2005-2, SLAC-R-771.

[67] S. Redaelli, “Stabilization of Nanometre-size Particle Beams in the Final Focus System

of the Compact Linear Collider (CLIC)", PhD Thesis, Université de Lausanne, 2003, 194 pages, also as CERN-AB-2004-025.
[68] B.Bolzon et al, "Study of supports for the final doublets of ATF2", Proceedings Nanobeam'08, May 25-30, 2008, Novosibirsk, Russia also LAPP-TECH-2008-04.
[69] P. Raimondi and A. Seryi, "Novel Final Focus Design for Future Linear Colliders", Phys. Rev. Lett. **86**, 3779-3782 (2001).
[70] H. Grote and F. Schmidt, "MAD-X - An Upgrade from MAD8", CERN-AB-2003-024, ABP.
[71] E. Forest, F. Schmidt and E. McIntosh, "Introduction to the Polymorphic Tracking Code", KEK Report 2002-3.
[72] F. Zimmermann et al., "Final-Focus Schemes for CLIC at 3 TeV", Proc. 18th International Conference on High Energy Accelerators (HEACC2001), Tsukuba, Japan, CERN-SL-2001-010 AP and CLIC Note 476 (2001).
[73] J.A. Nelder and R. Mead, Computer Journal, 1965, vol **7**, pp 308-313.
[74] D. Schulte, et al., "Simulation Package based on PLACET", PAC2001, Chicago (2001); CERN/PS 2001 028 (AE), CLIC Note 482 (2001).
[75] D. Schulte, et al., "Beam-Beam Simulations with GUINEA-PIG", ICAP98, Monterey, CA., USA (1998).